

RUPRECHT 147: THE OLDEST NEARBY OPEN CLUSTER AS A NEW BENCHMARK FOR STELLAR ASTROPHYSICS

JASON L. CURTIS^{1,2,3}, ANGIE WOLFGANG^{3,4}, JASON T. WRIGHT¹, JOHN M. BREWER⁵, AND JOHN ASHER JOHNSON⁶
ACCEPTED TO AJ: December 7, 2012

ABSTRACT

Ruprecht 147 is a hitherto unappreciated open cluster that holds great promise as a standard in fundamental stellar astrophysics. We have conducted a radial velocity survey of astrometric candidates with Lick, Palomar, and MMT observatories and have identified over 100 members, including 5 blue stragglers, 11 red giants, and 5 double-lined spectroscopic binaries (SB2s). We estimate the cluster metallicity from spectroscopic analysis, using Spectroscopy Made Easy (SME), and find it to be $[M/H] = +0.07 \pm 0.03$. We have obtained deep CFHT/MegaCam $g'r'i'z'$ photometry and fit Padova isochrones to the $(g' - i')$ and 2MASS $(J - K_S)$ CMDs, using the τ^2 maximum-likelihood procedure of Naylor (2009), and an alternative method using 2D cross-correlations developed in this work. We find best fits for isochrones at age $t = 2.5 \pm 0.25$ Gyr, $m - M = 7.35 \pm 0.1$, and $A_V = 0.25 \pm 0.05$, with additional uncertainty from the unresolved binary population and possibility of differential extinction across this large cluster. The inferred age is heavily dependent by our choice of stellar evolution model: fitting Dartmouth and PARSEC models yield age parameters of 3 Gyr and 3.25 Gyr respectively. At ~ 300 pc and ~ 3 Gyr, Ruprecht 147 is by far the oldest nearby star cluster.

Subject headings: open clusters: general — open clusters: individual (Ruprecht 147)

1. INTRODUCTION

The observational foundations of stellar astrophysics are studies of the Sun and stellar clusters. A few “benchmark” clusters form the basis of our understanding of stellar evolution, and the effects of abundance, age, and mass on stars. When fully characterized with precise ages, distances and metallicities, these clusters become touchstones for similar stars in the field and test models of stellar evolution and structure.

Galactic gravitational tidal forces are effective at disrupting most Galactic clusters on a time scale of a few hundred Myr (Soderblom 2010), so most clusters tend to be relatively young. This is fortunate for studies of early stellar evolution and massive stars: for such work stellar astrophysicists have access to several nearby young clusters (e.g. Pleiades $\sim 100 - 200$ Myr; Hyades and Praesepe ~ 700 Myr).

Studies of the older cool stars (age $\gtrsim 1$ Gyr) that typify the field must rely on rarer and thus more distant clusters. Studies of the typical rotation, activity level, and photometry of G, K and M dwarfs as a function of age and mass, such as the WIYN Open Cluster Survey (WOCS⁷), the Palomar Transient Factory (PTF, Agüeros et al. 2011) and the *Kepler* Cluster Study (Meibom et al. 2011), investigate clusters with distances of 1 – 4 kpc. These larger distance moduli can make spectroscopic study of their low mass members extremely

difficult.

Fortunately, Dias et al. (2001) and Kharchenko et al. (2005) used catalog data to identify Ruprecht 147 (R147 = NGC 6774), and estimated its age to be ~ 2.5 Gyr at a distance of 175 – 270 pc, making R147 by far the oldest nearby cluster⁸ (e.g. WEBDA lists NGC 752 at 1.1 Gyr and 457 pc, Figure 1).

1.1. Pre-2000 literature

Despite its promising scientific potential due to the unique combination of its age and distance, and despite having a similar distance and size to Praesepe, R147 was completely overlooked by stellar astronomers until the works by Dias et al. and Kharchenko et al.. This is likely because its proximity makes R147 a very sparse cluster on the sky: there are only ~ 50 members with $V < 11$ and only ~ 10 with $V < 9$ spread over 5 square degrees. Its presence is also obscured by its location in the Galactic plane ($-14^\circ < b < -12^\circ$, in Sagittarius), and the fact that due to its age, it lacks the many bright A stars that made similarly nearby clusters so obvious, even to the astronomers of antiquity.

In fact, a complete pre-2000 bibliography of R147 consists almost exclusively of entries in various catalogues. R147 was originally discovered in 1830 by John Herschel, who described it as “a very large straggling space full of loose stars” (Herschel 1833), and labelled it GC 4481 (Herschel 1863). Since then it has appeared with numerous designations including NGC 6774, OCL 65, Lund 883 (Dreyer 1888; Alter et al. 1958; Lynga & Palous 1987;

⁸ One WEBDA cluster, Loden 1, is plotted as an open circle in Figure 1, and has properties that are apparently similar to Ruprecht 147. The membership and properties of Loden 1 were determined by Kharchenko et al. (2005). They identify only nine $1-\sigma$ members from proper motions and photometry, and none have measured radial velocities. The Loden 1 grouping has not been confirmed as a real open cluster, and the properties derived by the automated search of Kharchenko et al. (2005) are thus unreliable.

¹ Department of Astronomy & Astrophysics, The Pennsylvania State University, University Park, PA 16802, USA

² jcurtis@psu.edu

³ NSF Graduate Research Fellow

⁴ Department of Astronomy & Astrophysics, University of California, Santa Cruz, CA 95064, USA

⁵ Department of Astronomy, Yale University, New Haven, CT 06511, USA

⁶ Department of Astrophysics, California Institute of Technology, Pasadena, CA 91125, USA

⁷ <http://www.astro.wisc.edu/wocs/>

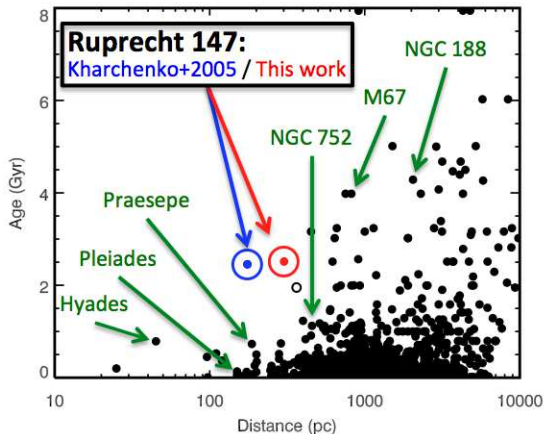


Figure 1. Data from the WEBDA database (Mermilliod & Paunzen 2003) showing all known clusters in distance – age space. R147 is by far the oldest nearby cluster, and holds great promise as a standard in fundamental stellar astrophysics: Kharchenko et al. (2005) values shown in blue, ours in red. WEBDA lists an age for M67 at 2.5 Gyr, but we plot it at 4 Gyr according to Pichardo et al. (2012) and references therein. The open circle next to R147 denotes Loden 1, an unconfirmed grouping of stars with unreliable properties – see footnote 8 for a discussion.

Mermilliod 1995). Some star charts have even designated R147 as an asterism, and not a true cluster (e.g. “Burnham’s Celestial Handbook: An Observer’s Guide to the Universe Beyond the Solar System” lists NGC 6774 as “possibly not a true cluster” (Burnham 1966)). The name we use here originates from Ruprecht (1966), who classified R147 as a III-2-m cluster in the Trumpler system (Trumpler 1930, 160). According to Archinal & Hynes (2003), Brian Skiff realized that NGC 6774 and R147 are likely the same star cluster. Archinal & Hynes (2003) describe R147 as a “45’ sized V-shaped group of bright stars” that is “a sparse possible open cluster”, and estimate the cluster center as the location of HD 180228 (while this star’s photometry apparently places it on the R147 red giant branch, the Tycho-2 proper motions, -1.6 and -6.3 mas/yr in right ascension and declination, are inconsistent with cluster membership, see Figure 3). Figure 2 highlights our high-confidence members on an optical image. Herschel’s cluster identification is truly amazing, given the lack of a well defined cluster core. But those arguing for the asterism status were not entirely wrong either: of the 51 stars with $V < 9$ within $\approx 2^\circ$ of the cluster center, we confirm only 11 as members.

1.2. Recent work in the literature

Only in the last decade has R147 received any individual attention in studies of open clusters. Dias et al. (2001) first identified R147’s membership based on the stellar population’s common proper motion: selecting stars in the Tycho-2 Catalogue (Høg et al. 2000) that were spatially coincident with BDA clusters (The Open Cluster DataBase, Mermilliod 1995), they determined cluster membership with the Tycho-2 proper motions using the statistical method of Sanders (1971) and found 33 stars with mean proper motion of $\mu_\alpha = -0.8 \pm 2.3$ and $\mu_\delta = -28.5 \pm 2.3$ mas/yr. Dias et al. (2001) also provided the first distance estimate based on only two Hippar-

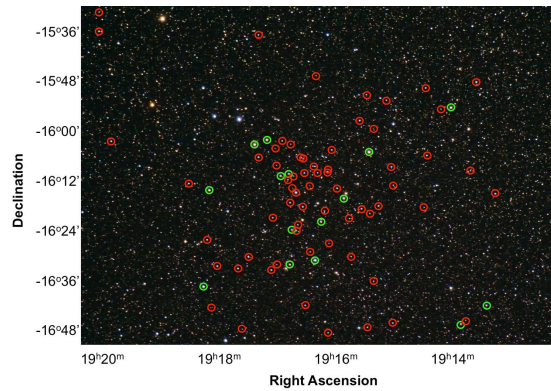


Figure 2. This astrophotograph of a portion of the Ruprecht 147 field was taken and kindly provided by Chris Beckett and Stefano Meneguolo of the Royal Astronomical Society of Canada. We have attached an approximate coordinate system solution (we have not solved for the field distortions) and circled the 80 high-confidence members in red. There are 52 stars in this image with $V < 10$, and only 17 are members of R147 and are circled green. Of the 47 stars with $V < 9$ within $\approx 2^\circ$ of the cluster center (extending beyond this image), only 11 are members. It is remarkable that Herschel correctly identified this as an open cluster in 1830.

cos parallax measurements⁹ (HIP1, Perryman & ESA 1997): $\pi = 3.57 \pm 1.01$ mas (280 ± 79 pc) for HIP 94635 (CWW 1)¹⁰, and 3.75 ± 1.04 mas (267 ± 74 pc) for HIP 94803 (CWW 2), which they average to 3.7 ± 0.2 mas, estimating the distance to R147 to be 250 pc¹¹. Since then, van Leeuwen (2007a) (HIP2) has performed a new data reduction and issued an updated catalog with parallaxes of 5.48 ± 0.65 mas (182 ± 22 pc) for HIP 94635, and 4.92 ± 0.79 mas (203 ± 33 pc) for HIP 94803¹².

Dias et al. (2002) compiled all available data for 2095 galactic clusters (*The New Catalogue of Optically Visible Open Clusters and Candidates*, or DAML02) and published an updated membership list and cluster properties for R147: 25 members, proper motion $\mu_\alpha = -0.9 \pm 0.3$ and $\mu_\delta = -29.3 \pm 0.3$ mas/yr, $RV = 41$ km s⁻¹ (from the single published measurement in Wilson (1953), see §3.2), distance = 200 pc, color excess $E(B - V) = 0.2$ mag., and an age 3.2 Myr (presumably from misidentifying blue stragglers as main sequence turnoff stars). Dias et al. re-classified R147 as IV-2-p (Trumpler system).

Following their 2002 work, Dias et al. (2006) selected all clusters in their DAML02 catalogue with known distances and queried the UCAC-2 catalogue (Zacharias et al. 2004b) for all stars within the mea-

⁹ Actually, three R147 members appear in the Hipparcos catalog, see §4.7

¹⁰ Throughout this paper, we will refer to individual stars with the designation “CWW #” (CWW = Curtis, Wolfgang and Wright). Our membership list provides 2MASS IDs, astrometry, photometry, radial velocities, and membership probabilities for 108 stars. The CWW ID numbers sort these stars according to V magnitude (see Table 6).

¹¹ although this is a numerical error as $1000 / 3.7 = 270$, not 250.

¹² van Leeuwen (2007b, §3.3.1, 3.3.2) cautions against deriving distances and distance moduli from parallaxes when the relative error is greater than 10%. The Lutz-Kelker bias can also introduce a 0.1 magnitude systematic offset at 10% relative error

sured cluster radii, plus $2'$, of their tabulated cluster centers. Employing similar methods as Dias et al. (2001), they derived a mean proper motion for R147 of $\mu_\alpha = -4.6 \pm 0.4$ and $\mu_\delta = -5.6 \pm 0.4$, and identified 200 cluster members. Figure 3 shows the proper motions for stars in the R147 field, color-shaded by membership probability as derived by Dias et al. (2006). The black circle highlights the proper motion of R147 according to Kharchenko et al. (2005) and confirmed in this work, and shows that the Dias algorithm missed the cluster, locating the field stars instead. The Dias et al. (2006) membership list and cluster parameters are thus unreliable. Dias et al. (2006) attribute their algorithm’s failure to the large angular size of R147.

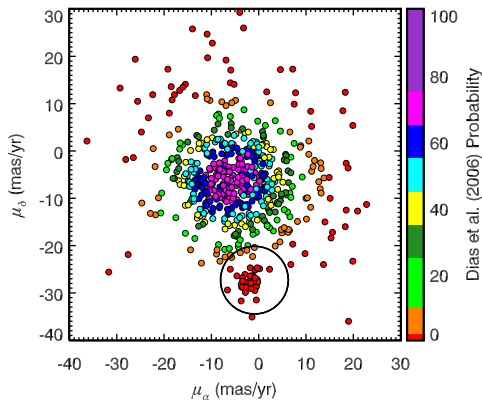


Figure 3. Proper motion diagram of stars in the R147 field, color shaded by membership probability as derived by Dias et al. (2006). The black circle highlights the proper motion of R147 (Kharchenko et al. 2005, and confirmed here). The Dias membership probabilities are clearly in error.

A similar automated effort has been undertaken by Kharchenko (2001), who assembled the All-Sky Compiled Catalogue of 2.5 Million Stars (ASCC-2.5), including proper motions from the Tycho-2 catalog (Høg et al. 2000), Johnson BV photometry, and radial velocities and spectral types when they are available.

Kharchenko et al. (2005) searched this catalog and identified 520 Galactic open clusters, including R147. Their algorithm determined the core and cluster angular radii, and the distances, mean space motions (proper motion and radial velocity), and ages of the clusters. Three important differences exist between the Dias et al. (2006) membership and properties and those of Kharchenko et al. (2005): (1) Kharchenko et al. correctly identify the cluster, cataloging 41 $1\text{-}\sigma$ members; (2) they provide the first reliable age estimate of 2.45 Gyr from their isochrone fitting; and (3) they claim a new distance of only 175 pc, 75 pc closer than that inferred from the original Hipparcos parallaxes, but similar to the distances derived in HIP2. While we determine a similar age of ~ 2.5 Gyr, we derive a distance $d \approx 300$ pc (§4.3, 4.4) by fitting isochrones to a spectroscopically derived $T_{\text{eff}} - \log g$ diagram, and 2MASS ($J - K_S$) and CFHT/MegaCam ($g' - i'$) color – magnitude diagrams. Figure 4 plots the CMD used by Kharchenko et al. (2005) to derive age and distance. The

Tycho-2 BV photometry is magnitude limited at $V \sim 11$, near the R147 main sequence turnoff. ASCC-2.5 is supplemented with various ground based photometry for fainter magnitudes, which Figure 4 demonstrates is insufficient for main sequence fitting. While the MSTO provides a strong constraint on the age, the discrepancy between our derived distance and that of Kharchenko et al. can be explained by the ill-defined $(B - V)$ main sequence. Their analysis was also hindered by a lack of a spectroscopically determined composition, and they assumed Solar metallicity. Without an accurate metallicity, and with a main sequence dominated by photometric error, it is difficult to disentangle visual extinction, age, composition and distance. Instead, Kharchenko et al. (2005) assumed $A_V = 0.465$ from the Schlegel et al. (1998) dust map at their location for the cluster center, even though according to this dust map A_V varies from 0.3 to 0.6 mag. across the cluster (see §4.1). Although Dias et al. (2001) were the first to determine the distance, Schilbach et al. (2006) were the first to discuss Ruprecht 147 specifically as an old nearby cluster in a peer-reviewed publication.

Despite these issues, the works of Dias et al. and Kharchenko et al. are significant because they essentially re-discovered Ruprecht 147 and provided the first good evidence that R147 is in fact the oldest nearby star cluster.

Most recently, Pakhomov et al. (2009) observed three cluster red giants and spectroscopically measured radial velocities and stellar properties (discussed in §3.2, 4.2). They determined the cluster metallicity to be super-Solar, thereby decreasing the estimated age, from a fit to an enriched Padova isochrone (Girardi et al. 2000; Marigo et al. 2008)¹³ to ~ 1.25 Gyr, and derived a distance of 280 ± 100 pc, along with a color excess of $E(B - V) = 0.11$ (or $A_V = 0.34$, assuming $R_V = 3.1$).

Ruprecht 147 has also appeared in the open cluster luminosity function study of Elsanhoury et al. (2011) and a paper on Galactic kinematics and structure as defined by open clusters by Zhu (2009), but these works undoubtedly suffer from a poorly determined membership and uncertain cluster properties.

We have begun an observational campaign to characterize R147, catalog its members, and prove its benchmark status. Here we present our initial efforts, detailing in particular our R147 membership search that more than doubles the number of known cluster members (§3), and our derivation of the cluster’s age, distance, and metallicity (§4). We begin with an overview of our photometric and spectroscopic datasets.

2. OBSERVATIONAL DATASETS

Cluster members are identified by their common space motion, determined from proper motions and radial velocities, and by their placement on a color – magnitude diagram (CMD). We utilize the NOMAD, UCAC-3 and PPMXL astrometric catalogs for proper motions. We have high resolution, single order echelle spectra from

¹³ The Padova isochrones are available at <http://stev.oapd.inaf.it/cgi-bin/cmd>. We primarily use these stellar evolution models because the Padova group provides synthetic photometry in a large number of systems, including the CFHT/MegaCam $g'r'i'z'$ filter set allowing us to analyze our optical photometry.

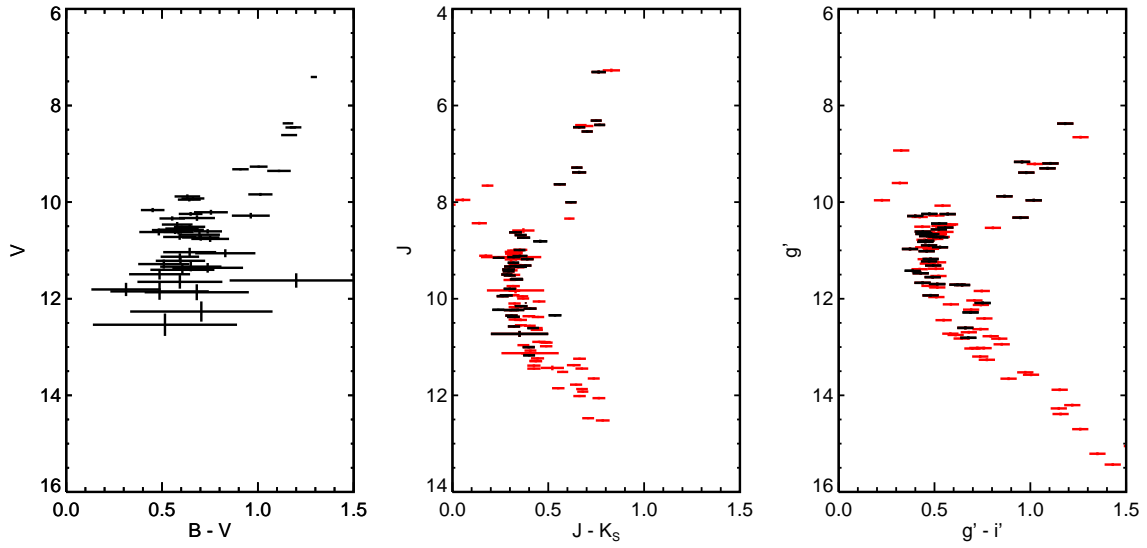


Figure 4. Ruprecht 147 color – magnitude diagrams. The left panel shows the $(B - V)$ photometry used by Kharchenko et al. (2005) to estimate age and distance by isochrone fitting. These data are magnitude limited at the main sequence turnoff. The central and right panels plot the same stars in black, along with our additional members in red. The main sequence is better defined in the 2MASS NIR ($J - K_s$) and our optical ($g' - i'$) CMDs, which explains the $\approx 80\%$ discrepancy between the Kharchenko et al. distance of 175 pc and our value of ≈ 300 pc. The g' and i' error bars are set at 0.03 magnitude. The color errors are the magnitude errors added in quadrature.

MMT Observatory; and high-resolution, cross-dispersed echelle spectra from Lick, Palomar, and Keck Observatories. We acquired deep $g'r'i'z'$ photometry of a 4 square degree field with CFHT/MegaCam, and utilize NIR JHK_S photometry from the 2MASS Point Source Catalog. Other observing projects are underway, including deep NIR imaging with UKIRT/WFCAM (PI Adam Kraus), a 250 ks exposure of the cluster core with Chandra/ACIS (PI Steve Saar), and an RV survey for K and M dwarf members with Magellan/MIKE+MagE (PI Steve Saar).

2.1. Astrometric catalogs

Our initial list of candidate members was drawn from the NOMAD and UCAC-3 catalogs. The Naval Observatory Merged Astrometric Dataset (NOMAD, Zacharias et al. 2004a) combines data (positions, proper motions, and BVR/JHK photometry) for over 1 billion stars from the Hipparcos (Perryman & ESA 1997), Tycho-2 (Høg et al. 2000), UCAC-2 (Zacharias et al. 2004b), USNO-B1.0 (Monet et al. 2003), and 2MASS (Skrutskie et al. 2006) catalogs. The Third USNO CCD Astrograph Catalog (UCAC-3, Zacharias et al. 2009) expands on NOMAD by improving UCAC-2 in many ways, including complete sky coverage, reduced systematic errors for CCD observations, deeper photometry ($R \approx 8 - 16$) for ~ 80 million stars, and improved astrometry (resolved double stars, inclusion of several new catalogs, and re-reduction of early epoch photographic plates to derive proper motions).

In this paper, we use proper motions from the PPMXL catalog (Roesser et al. 2010), and provide these values in Table 6. PPMXL utilizes astrometry from the USNO-B1.0 and 2MASS catalogs to calculate proper motions in the ICRS system for approximately 900 million objects, including ~ 410 million with 2MASS photometry. The catalog covers the entire sky down to $V \approx 20$. PPMXL was released in 2010, after we had derived our initial membership catalog. Some stars have NOMAD and/or UCAC-3 proper motions consistent with cluster membership, but are discrepant according to the PPMXL values (and vice versa). We include these stars in our membership list despite this, and we evaluate their probability of membership based on all available kinematic and photometric data (§3).

2.2. Lick 3-m and Palomar 200-in spectra and radial velocities

We performed initial radial velocity confirmation of suspected members to verify the existence of the cluster with the Hamilton echelle spectrometer on the 120 inch Shane telescope at Lick Observatory ($R \sim 50,000$; Vogt 1987). Our objectives were to obtain RVs of known and suspected members, to identify new members, and to obtain high resolution spectra of the brightest members at high signal-to-noise ratios (SNRs) for more detailed analysis of abundances and chromospheric activity.

We observed candidate cluster members on UT 2007 July 31 – August 1 and 2007 August 22 – 23, including the members identified by Kharchenko et al. (2005). To locate additional candidate members, we selected stars from the NOMAD catalog that were within $1^\circ.25$ of the published cluster center and that had UCAC-2 and TYCHO-2 proper motions within 5 mas/yr of

the Kharchenko et al. value. Although there are over 750,000 NOMAD stars in the field due to its large size and location in the Galactic plane, the cluster is separated enough from the field in proper motion space that this yielded a list of 1348 stars, illustrated in Figures 5.

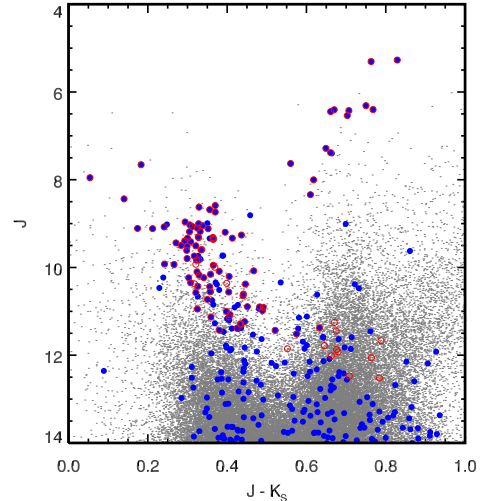


Figure 5. Proper motion cuts made to NOMAD stars to identify candidate R147 members. Of the over 750,000 NOMAD stars in the $1^\circ.5$ radius region centered on R147, 38,623 have $0 < J - K_S < 1$ and $4 < J < 14$ which are shown in gray. There are 1348 stars with NOMAD proper motions within 5 mas/yr of the cluster value, 280 of which have $J < 14$ and are plotted in blue. Our final membership list of 108 stars are circled in red. This plot demonstrates that there is really only one obvious sequence at bright magnitudes where the proper motions are reliable, including a well-defined red giant branch.

To further vet this list, we used NOMAD ($B - V$) and 2MASS ($J - K_S$) color - magnitude diagrams to identify stars consistent with an assumed distance of 230 pc, a compromise between the HIP1 distance to the cluster (270 pc) and the value of Kharchenko et al. (175 pc). We combined the CMDs and proper motion information to estimate crude membership probabilities based on the Hipparcos main sequence with no reddening corrections, calculated generously to account for uncertainties in the cluster parameters and for the poor quality of some of the NOMAD proper motion entries, and we favored brighter targets to improve the efficiency of vetting candidate members at the telescope.

We drew from this list, sorted by membership probability, to choose targets for spectroscopic study at Lick Observatory. We used these spectra to measure radial velocities for the stars and determine the space motion of the cluster.

2.2.1. Data acquisition and raw reduction

We adopted the spectrograph setup procedure of the California and Carnegie Planet Search, which placed bright emission lines from a thorium-argon (ThAr) lamp on specific pixels to approximately reproduce a known wavelength solution to a fraction of a pixel. Our prior experience using the Hamilton spectrograph at coude focus revealed that the wavelength solution is reliable to a pixel or two over the course of the night. This was

sufficient for our purposes of measuring radial velocities to $< 5 \text{ km s}^{-1}$, a precision which allows most interloping field stars to be identified, so we did not attempt any further wavelength calibration throughout the night. In practice, our radial velocity accuracy proved to be much better than 5 km s^{-1} .

Observing conditions were good, and we obtained several high SNR spectra of radial velocity standard stars of various spectral types throughout the nights, chosen from the catalog of Nidever et al. (2002). For candidate members we used exposure times of 60–90 s, depending on the magnitude of the star. For fainter stars we obtained SNRs as low as 1 per pixel, which is sufficient for our velocity work because of the broad spectral coverage of the Hamilton spectrograph. This strategy allowed a large number of stars to be observed in our allocated time for this low-declination cluster, which only spent a few hours per night at sufficiently low airmass to be useful.

The raw spectra were processed with the standard Hamilton Spectrograph data reduction pipeline used for precise radial velocity work by the California and Carnegie Planet Search, which includes bias subtraction and flat fielding of each frame and which results in a one-dimensional spectrum for each of 92 orders.

We calculated an empirical blaze function for each order by fitting a polynomial to the spectra of several rapidly rotating B stars that we observed for this purpose. These stars show no high resolution spectral features, and we corrected orders contaminated by the effects of the broad Balmer lines by averaging the polynomial blaze function of the neighboring orders. Variations in slit illumination from target to target created apparent continuum variations that were not perfectly removed by this process, and the nature of the polynomial fitting process caused the fit to diverge from the actual spectrum significantly at the edges of orders. The resulting spectra were nonetheless sufficiently flat that the cross correlations required for our data analysis (§2.2.3) could be confidently performed.

2.2.2. Palomar spectra

We followed a similar procedure at Palomar Observatory to determine membership probabilities and activity measurements of fainter candidate members. Target stars were drawn from the same sorted list that was compiled for the Lick observing run the previous year, including 25 targets that were chosen for follow-up observations based on qualitative examination of the radial velocity measurements derived from the Lick data, either because the signal-to-noise ratio of the Lick data was too low for a definitive velocity measurement or the star showed evidence of binarity, necessitating a second epoch.

We observed on 2008 August 5 and 18 with the East-Arm Echelle ($R \sim 33,000$; Peri 1995) on the Hale 200-inch at Palomar, following our earlier procedure of short integrations at very low signal-to-noise ratio (the additional aperture of the 200-in over the 3-m, somewhat mitigated by the low throughput of the East Arm Echelle, allowed us to explore fainter targets, or brighter targets at better SNR).

2.2.3. Radial velocity determination

Although we adopted the rough wavelength calibration used for planet search work, we did not attempt to use this calibration to measure our radial velocities. Rather, we extracted radial velocities in pixel space by cross-correlating the spectra of our candidate cluster members with those of our observed RV standard stars (a similar pixel-space cross-correlation method was employed by Norris et al. (2011)). To reduce the errors introduced by comparing two stars of different spectral types, we paired each candidate member to an RV standard star that minimized the difference between their $V - J$ colors ($\Delta(V - J)$), with $V - J = 0.8$ for the bluest standard star and $V - J = 2.4$ for the reddest.

Imperfect flat fielding produced a sharp spike at exactly zero shift in the cross-correlation functions (CCFs), and the presence of telluric lines created a narrow peak there, complicating the radial velocity measurements derived from these CCFs. This justified our use of velocity standard stars as cross-correlation templates rather than high SNR spectra of actual cluster members, since the standards have different radial velocities than the cluster and so the true CCF peak is far removed from the spurious peaks at zero shift. To further address the problem of telluric lines, we empirically rejected those portions of the spectrum where these lines dominated the CCF: after dividing each of the 92 orders into three segments, we discarded from all spectra those segments that showed strong telluric peaks near zero shift.

Computing these CCFs for the different combinations of RV standard stars with $\Delta(V - J) < 0.5$ allowed us to calibrate the conversion from pixel space shifts to radial velocities, after applying a barycentric radial velocity correction. This calibration step thus obviates the need for a transformation into wavelength space. Specifically, we fit a linear function with zero intercept to the measured RV standard stars' CCF pixel shifts as a function of the difference in their radial velocities, giving us the velocity shift per pixel in each spectrum segment. The root mean squared of the residuals of this fit is less than 0.6 km s^{-1} ; this provides our best measure of the systematic velocity precision we expect at high SNRs.

Comparison of this calibration constant among the segments confirmed that the velocity shift per pixel of the Hamilton spectrograph is nearly constant for each of the 92 orders. This is not surprising given that both the resolution, R ($= \lambda/\Delta\lambda$ per resolution element), and the sampling, s (pixels/resolution element), are nearly constant across an echellogram, and that our calibration constant, having units of $\text{km s}^{-1}/\text{pixel}$, is essentially c/Rs , where c is the speed of light. This allowed us to add the CCFs of the remaining segments together to improve the SNR of the stellar signal, and enabled the clear identification of a peak and its associated pixel shift in the combined CCF. To be conservative, we divided each spectrum into three sets of segments, corresponding to the left, middle and right sides of each order. After separately summing the CCFs in each set, we required that the location of the tallest peak in the summed CCFs to be identical in all three sets; however, when the side segments produced noisy CCFs, as was the case for stars with $\text{SNR} \sim 10$, we used the location of the tallest peak in the middle segments' summed CCF, as long as the peak met our high quality classification.

We visually inspected each CCF produced by our procedure and classified the stars into two categories based on the quality of their CCFs: either the combined CCF had one clear peak, which corresponded to high SNR spectra, or the combined CCF had multiple peaks of approximately equal height, which indicated that the CCF was dominated by noise, and which usually corresponded to spectra with SNR $\lesssim 2$ per pixel (some of these discarded stars were later revisited in the Palomar observing run in order to acquire higher SNR spectra).

We found a clear clustering of barycentric velocities near 43 km s^{-1} , which is within 2 km s^{-1} of the cluster RV quoted by Dias et al. (2002) that was based on a single measurement of a single putative member (§3.2). Upon closer inspection of the Lick velocities for signs of systematics, we found that these apparent cluster members' velocities exhibited a slight correlation with time from the beginning of the observing run to the end, with magnitude $2 - 4 \text{ km s}^{-1}$. We fit this trend to a linear function and removed it. We have also observed 49 of these stars with MMT/Hectochelle (with very high signal-to-noise ratio, we expect all to have RV precision $\approx 0.5 \text{ km s}^{-1}$, §2.4), and measure differences between the Lick/Palomar and Hectochelle RVs as large as 5 km s^{-1} , except for a possible single-lined spectroscopic binary (SB1) with a difference of 20 km s^{-1} . We interpret this offset between telescopes and spectrographs as a measure of systematic error in our absolute barycentric radial velocities.

Figure 8 illustrates the resulting RVs and shows a clear clustering around the cluster velocity. We tentatively identified as cluster members any stars with a measured radial velocity between 32 and 54 km s^{-1} , or roughly twice the typical systematic error.

2.3. Spectra from Keck/HIRES

Spectra of four cluster members were obtained on 2008 September 12 and 18 and for two members on 2011 October 17 with the High Resolution Echelle Spectrometer (HIRES, Vogt et al. 1994) on the 10-m telescope at Keck Observatory. The stars were kindly observed by the California Planet Survey team (CPS¹⁴) without an iodine cell, and with the B5 decker (slit of $3.5''$ length and $0.861''$ width), giving a typical resolution $R \sim 50,000$ in the $3360 - 8100 \text{ \AA}$ bandpass. Exposure times were monitored with a photomultiplier tube exposure meter to ensure high signal-to-noise ($S/N \sim 50 - 100$). These observations are summarized in Table 1, and were reduced by the standard CPS pipeline. Chubak et al. (2012) measured absolute radial velocities (results discussed in §3.2) and we derive stellar properties in Section 4.2.

2.4. Spectra from MMT/Hectochelle

We obtained high-resolution spectra with MMT/Hectochelle in the vicinity of the Ca II H & K lines for 48 members (as determined from Lick/Palomar RVs), 10 candidate members (from astrometry and photometry alone), and 23 potential astrometric reference stars. These data provide radial velocities, chromospheric activity indicators (e.g. (Wright et al.

2004)), and gravity diagnostics (via the Wilson-Bappu effect, Wilson & Vainu Bappu 1957) useful for identifying background giants as astrometric references. The remaining fibers not allocated for sky subtraction were assigned to proper motion candidates with inconsistent photometry to assess how R147 members are kinematically distinct from the field.

MMT is a 6.5-m telescope located at the Fred Lawrence Whipple Observatory on Mt. Hopkins, AZ (Fabricant et al. 2004). Hectochelle is a high-resolution ($R \sim 32,000 - 40,000$) fiber-fed spectrograph, which provides simultaneous observations for 240 targets in a one square degree field (Szentgyorgyi et al. 1998; Fűrész et al. 2008). We observed the central square degree with the 'Ca41' Ca II H & K filter with 1×1 on-chip binning. Eight total hours were obtained to ensure sufficient signal-to-noise for a future chromospheric activity study. All observed targets have $g' = 9 - 15.5$.

Twelve 40-minute exposures were obtained over the nights of UT 2010 July 4 - 5. These data were reduced with an IRAF¹⁵-based automated pipeline developed at the Harvard-Smithsonian Center for Astrophysics, provided and run by Gabor Fűrész and Andrew Szentgyorgyi, which flat-fielded, cosmic-ray removed, and wavelength calibrated our targets and sky flats. The wavelength solution was determined from Thorium-Argon (ThAr) lamp comparison spectra, with an RMS precision of $0.2 - 0.5 \text{ km s}^{-1}$ (for reduction details, see Mink et al. 2007).

Radial velocities were measured by cross-correlating the target spectrum with Solar spectra obtained from the sky flat exposures, then corrected for Earth's heliocentric motion. We checked the fiber-to-fiber and day-to-day stability of the spectrograph by measuring velocity shifts determined by cross-correlating matched ThAr, Solar, and target spectra. The fiber-to-fiber velocity shift on the first night was $12 \pm 35 \text{ m s}^{-1}$ (for the ThAr spectra) and $200 \pm 200 \text{ m s}^{-1}$ (for the Solar spectra). We also measure a night-to-night variation between each fiber of $31 \pm 41 \text{ m s}^{-1}$ (ThAr) and $200 \pm 180 \text{ m s}^{-1}$ (Solar). The RVs measured each day for R147 stars show a mean absolute difference of 0.23 km s^{-1} . In summary, fiber-to-fiber and day-to-day offsets and errors are well under or comparable to the precision set by the wavelength solution. The RV distribution for 49 member stars is shown in Figure 8, and is discussed in §3.2.

2.5. Preliminary optical photometry

We imaged a 4 square degree field in the optical $g'r'i'z'$ bands in 2008 April and May with CFHT/MegaCam (Hora et al. 1994)¹⁶. With MegaCam's one square degree field of view, four fields were required to cover the majority of the known cluster. The fields are outlined over a 2MASS J band mosaic image in Figure 6. Six additional surrounding fields were imaged solely in i' band, for the purpose of first-epoch astrometry for the entire cluster, including any extended halo. We obtained both a series of short (1 second) and long (few minutes) ex-

¹⁵ IRAF is distributed by the National Optical Astronomy Observatories, which are operated by the Association of Universities for Research in Astronomy, Inc., under cooperative agreement with the National Science Foundation.

¹⁶ <http://www.cfht.hawaii.edu/Instruments/Imaging/MegaPrime/>

¹⁴ <http://exoplanets.org/cps.html>

Table 1
Keck/HIRES observations.

CWW ID	2MASS ID	Obs Date JD	Exposure Time seconds	Airmass	V^a mag.	S/N ^b	Notes ^c
72	19165800-1614277	2008-09-12	210	1.43	11.52	50	G dwarf / SB2
78	19160879-1524279	2008-09-12	170	1.44	11.82	60	late F dwarf
21	19132220-1645096	2008-09-18	90	2.17	9.98	80	Subgiant
22	19172382-1612488	2008-09-18	93	2.12	10.04	70	mid-F MSTO / SB1
44	19164495-1717074	2011-10-17	167	1.39	10.61	80	mid-F dwarf MSTO
91	19164725-1604093	2011-10-17	822	1.32	12.39	50	early G dwarf

^a V magnitudes are drawn from the NOMAD catalog.

^b Signal-to-noise ratio measured in the spectral order encompassing the Mg b triplet, in the 5034 – 5036 Å continuum.

^c Approximate classification, performed by matching spectroscopic and photometric properties to isochrone masses (§3.3). SB1 status suggested by inconsistent RVs from multiple epochs; MSTO = main sequence turnoff

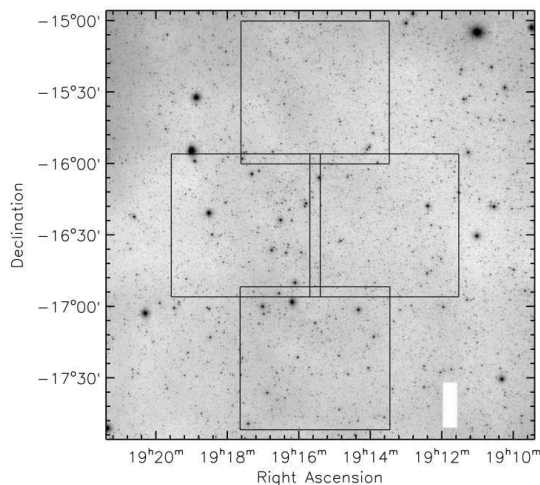


Figure 6. The four fields we imaged in $g'r'i'z'$ with CFHT/MegaCam, overlaid on a 2MASS J band mosaic image generated with Montage (<http://montage.ipac.caltech.edu>). We log-scaled and smoothed the image with a $3''$ boxcar.

posures in queued service observing mode. Typically, 5 dithered exposures were obtained for each field and exposure time.

These observations were pre-processed at CFHT with the Elixir pipeline (Magnier & Cuillandre 2002)¹⁷. Elixir creates master bias, dark and flat images, which are used to detrend the observation frames. SExtractor identifies sources and determines their pixel coordinates and raw flux. The astrometric calibration is performed by comparison to the USNO-B1.0 catalog.

Photometric magnitudes are calibrated from the instrumental magnitude with the application of a zero point, an airmass term and a color term. The coefficients are derived from observations of standard stars. Every night, one Landolt (1992) field was observed (SA-101, SA-107 and SA-113), along with two spectrophotometric standards (i.e. an O star or white dwarf: Feige 110, GD 153, HZ 43, BD+28 4211) and at least one CFHTLS Deep field. The zero points for each frame were determined from 13 to 26 standards observed in 4 to 9 separate images during a run. Standards were not necessarily ob-

served in all the filters utilized on a given night, but the zero point scatter across an observing run for each filter ranged from 0.0073 to 0.0180, and is therefore quite stable. Frames obtained on photometric nights provide the means to calibrate observations taken under less transparent conditions (the image scaling is done by TERAPIX, see below). The zero points were determined after the application of the superflat, and therefore are valid for all 36 CCDs. The photometric and astrometric calibration data are stored in the FITS image headers, and the data transferred to the Canadian Astronomy Data Centre (CADC) in Victoria¹⁸.

TERAPIX performed the final photometric and astrometric reduction of our MegaCam imagery¹⁹. The TERAPIX pipeline (Bertin et al. 2002) takes the detrended images and the preliminary calibration from Elixir, and completes a final photometric and astrometric calibration and provides source merged catalogs. First the images are re-scaled: the photometry is analyzed in each overlapping frame, and the frames are re-scaled to the photometry in the image with highest flux per source, which is considered to be the least extinguished. The overlapping images are stacked and the sources are re-extracted. The TERAPIX pipeline co-addition and astrometric calibration modules are now maintained at AstrOmatic.net, and documentation for each can be found at the SWarp²⁰ and SCAMP (Bertin 2006, Software for Calibrating Astrometry and Photometry,)²¹ webpages.

TERAPIX handles the CFHT Legacy Survey reduction. The CFHTLS²² and TERAPIX's CFHTLS reduction²³ webpages provide additional details relevant to the final photometric and astrometric calibrations.

TERAPIX kindly provided us merged $g'r'i'z'$ source catalogs for each field and exposure duration. The short exposures saturate at $g' \approx 9.5$ and the long exposures saturate at $g' \sim 16$. Sources with $g' \sim 17 - 18$ have consistent photometric magnitudes in each catalog, and sources are detected down to $g' \sim 24$ in the long exposure catalog. We therefore have photometry covering $10 \lesssim g' \lesssim 24$.

Our faintest red giant branch member is $g' = 10.53$

¹⁸ <http://www1.cadc-ccda.hia-ihp.nrc-cnrc.gc.ca/cadc/>

¹⁹ TERAPIX is a data reduction center located at the Institut d'Astrophysique in Paris, France: <http://terapix.iap.fr/>

²⁰ <http://www.astromatic.net/software/swarp>

²¹ <http://www.astromatic.net/software/scamp>

²² <http://www.cfht.hawaii.edu/Science/CFHTLS/>

²³ http://terapix.iap.fr/article.php?id_article=383

¹⁷ <http://www.cfht.hawaii.edu/Instruments/Elixir/home.html>

and $i' = 9.73$. Given the saturation limit in each band at approximately 9.5, the majority of the red giant branch stars are saturated in g' and i' . We will include the optical RGB in our figures in this work, but with stars plotted with open circles to distinguish these data from the more reliable optical photometry for the rest of the membership.

We estimate the photometric error by making use of the overlapping regions between the four imaged fields (see Figure 6). We matched all stars in the overlap regions in our bright source catalog (short exposures), and find a total of 1575 unique sources with $g' < 18$. Figure 7 plots the mean versus standard deviation of g' for the 2 – 4 independent measurements, depending on the number of overlapping regions containing the source. We find a typical value of $\Delta_{g'} = 0.035$ mag., but this is probably larger than what should be assumed for the photometric precision across the field, because one of the sources usually lies very close to the edge of one of the fields, where the mosaic dithering is incomplete and the photometry less reliable.

We have identified a ≈ 0.15 mag. zero point error in the z' band, and the persistence of a low-frequency mode that was not removed by the flat fielding. Given these issues with z' -band, we cautiously analyze the $(g' - i')$ CMD and provide photometry in Table 5. We will first analyze our spectroscopic results and 2MASS photometry, before fitting isochrones to our optical data. We will show in Section 4.4 that essentially identical cluster properties are determined from these 3 data sets. This consistency suggests the g' and i' zero points are likely accurate.

The Elixir and TERAPIX pipelines were developed and have been successfully used to reduce similar MegaCam imaging for the CFHT Legacy Survey²⁴. Despite these quality assurances, we consider this photometry to be preliminary, and we are currently working to further validate the accuracy of the Elixir and TERAPIX calibration.

3. IDENTIFYING THE RUPRECHT 147 MEMBERSHIP

We identify stars as R147 members based on their common space motion and placement on a color – magnitude diagram. Our initial membership list is drawn from the NOMAD and UCAC-3 astrometric catalogs and subjected to radial velocity vetting. We queried NOMAD and UCAC-3 for stars within a radius of 2° of the cluster center. Stars were accepted as candidates if their proper motions (§2.1) were within 8 mas/yr of the cluster mean (see Figure 3 for a proper motion vector point diagram). We adopted the values of Kharchenko et al. (2005) for the cluster center and mean proper motion: $(\alpha [h:m:s], \delta [d:m:s]) = (19:16:40, -16:17:59)$ and $(\mu_\alpha, \mu_\delta) [\text{mas/yr}] = (-0.6, -27.7)$ – after we identified the highest confidence members, we recalculated these locations and note no significant change (Table 4).

Table 6 gathers data for 108 stars of interest. The first column provides a designation internal to this paper: CWW # (CWW = Curtis, Wolfgang and Wright). The stars are ordered according to increasing V magnitude (provided by NOMAD). The table also includes the 2MASS ID (and therefore RA and Dec position);

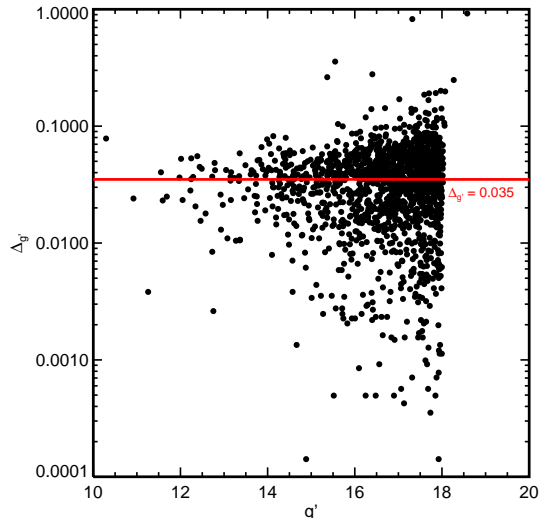


Figure 7. Photometric error estimates for CFHT/MegaCam $g'r'i'z'$ photometry: We imaged the R147 field with four separate but partially overlapping pointings (see Figure 6). We matched all stars in the overlap regions in our bright source catalog (short exposures), and find a total of 1575 unique sources with $g' < 18$. This figure plots the mean versus standard deviation of g' for the 2 – 4 independent measurements, depending on the number of overlapping regions containing the source. We find a typical value of $\Delta_{g'} = 0.035$, but this is probably larger than what should be assumed for the photometric precision across the field, because one of the sources usually lies very close to the edge of a field, where the mosaic dithering is incomplete, and so the photometry is less reliable.

PPMXL proper motions in mas/yr; the preliminary CFHT/MegaCam g' and $g' - i'$ optical photometry; 2MASS J and $J - K_S$ NIR photometry; and radial velocities RV_{LP} and RV_H (Lick/Palomar and Hectochelle, respectively). A membership probability is assigned to each of these data, according to criteria discussed below and summarized in Table 2, and is listed in the order: (1) radial distance in proper motion space from the cluster mean, (2) RV_{LP} , (3) RV_H , (4) proximity to cluster locus on the 2MASS $(J - K_S)$ CMD and (5) CFHT/MegaCam $(g' - i')$ CMD.

The derivation of quantitative membership probabilities is precluded by the large uncertainties in proper motion and our Lick/Palomar velocities, combined with the intrinsic spread in the R147 main sequence due to unresolved stellar multiplicity and the possibility of differential reddening, along with non-negligible photometric error.

Instead we designate three confidence levels: ‘Y’ for *yes this is consistent with cluster membership*, ‘P’ for *possible / probable member*, and ‘N’ for *not likely / non-member*. Each membership criterion is independently assessed and assigned a confidence level designation (whenever data are unavailable, a ‘-’ is assigned instead). The following sections address each criterion, and establish the ranges for each level (summarized in Table 2). The results from all fields are then reviewed and an overall membership confidence level is assigned to each star according to the same ‘Y’, ‘P’, ‘N’ scheme.

We find 81 stars of highest confidence, 21 stars with ‘P’ possible member status, and 6 stars with little to no probability of membership - at least as single star mem-

²⁴ For a list of publications, see <http://www.cfht.hawaii.edu/Science/CFHTLS/cfhtlspublications.html>

bers (multiple star systems could show RVs and photometry inconsistent with membership as we have defined it, while still being gravitationally bound members of R147).

3.1. Proper motion

We now primarily use PPMXL proper motions to assess membership, although our original membership list was derived from NOMAD and UCAC-3. The typical PPMXL errors range from 1 to 5 mas/yr in proper motion, and so we designate stars with proper motion within this 5 mas/yr of the cluster mean, as ‘Y’ members. Only stars within ~ 8 mas/yr were considered in our initial candidate list, and we found that the majority of bright candidates had velocities consistent with cluster membership. There are six stars that we had originally classified as ‘Y’ or ‘P’ according to their NOMAD proper motions, but which have PPMXL proper motions more than 8 mas/yr different than the cluster’s mean motion. Despite this large discrepancy from the PPMXL data, we classify these stars with conflicting proper motion data as ‘P’, and will consider their velocities and photometry when assigning their final probability.

3.2. Radial velocity

The General Catalogue of Stellar Radial Velocities (Wilson 1953) contains a single entry for a cluster member: HD 180015 (HIP 94635, classified as K0III, CWW 1). Wilson reported $RV = 41 \text{ km s}^{-1}$, with quality designation ‘C’, corresponding to a typical uncertainty = 2.5 km s^{-1} and maximum uncertainty = 5 km s^{-1} . This was the first and only available RV until Pakhomov et al. (2009) observed three other cluster red giants: HD 179691 (CWW 9) at 46.7 km s^{-1} , HD 180112 (CWW 10) at 40.1 km s^{-1} , and HD 180795 (CWW 7) at 40.8 km s^{-1} , with $S/N > 100$, and precision estimated at $0.5 - 0.8 \text{ km s}^{-1}$. The RV for HD 179691 is 6 km s^{-1} larger than the other two stars, too large to be explained by the cluster velocity dispersion, which implies this star is either a SB1 binary or a non-member. We observed these stars at Lick/Palomar and measure $RV_{LP} = 42.1, 41.4, 42.4 \text{ km s}^{-1}$, respectively. While our measurements for the second two stars are in basic agreement with Pakhomov et al. (2009), the velocity for HD 179691 now appears consistent with the cluster mean, supporting its membership and corroborating its SB1 status.

Chubak et al. (2012) have also measured RVs with rms errors $\sim 50 \text{ m s}^{-1}$ for our 5 single-lined Keck/HIRES spectra (Table 3). We list these here in km s^{-1} , with our Lick/Palomar velocities in parenthesis for comparison: CWW 44: $41.41 (42.2)$, CWW 91: $41.50 (42.8)$, CWW 21: $40.35 (41.9)$, CWW 78: $41.02 (40.8)$, and CWW 22: $46.63 (51.9)$. We followed up CWW 22 with Hectochelle and measure $RV = 38 \text{ km s}^{-1}$ on both nights, and classify it a SB1.

Selecting the six stars above showing no evidence of binarity, we find a typical cluster radial velocity of $40.86 \pm 0.56 \text{ km s}^{-1}$ (if we take only the 4 Keck stars analyzed by Chubak et al., then we find the cluster RV is $41.07 \pm 0.52 \text{ km s}^{-1}$). We take stars with RVs consistent with this value as high-probability cluster members. Figure 8 plots 98 stars with Lick/Palomar velocities (shown

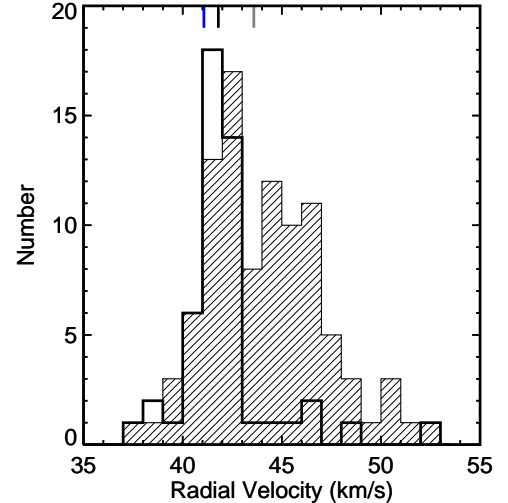


Figure 8. R147 radial velocity distribution. The gray hash designates RVs measured from Lick/Palomar (98 stars), with $RV_{LP} = 44 \pm 3 \text{ km s}^{-1}$. The black line plots 45 stars with Hectochelle velocities, $RV_H = 41.6 \pm 1.5 \text{ km s}^{-1}$. Tick marks on top indicate median values, color-coded to RV source: blue shows the cluster $RV = 41.07 \pm 0.52 \text{ km s}^{-1}$ from the 4 Keck stars (described in §3.2), gray and black represent Lick/Palomar and Hectochelle respectively. The width of each distribution is as expected from the RV precision of each survey, and should not be interpreted as a resolved cluster velocity dispersion. According to the quoted RV precision of Chubak et al. (2012), the 0.5 km s^{-1} dispersion in our 4 Keck velocities might actually be the intrinsic cluster velocity dispersion.

in gray hash) with $RV_{LP} = 43.8 \pm 3.2 \text{ km s}^{-1}$. Also shown are 45 stars with Hectochelle velocities (black line) with $RV_H = 41.6 \pm 1.5 \text{ km s}^{-1}$. The blue tick mark at the top shows the typical cluster velocity from above at 40.57 km s^{-1} . The width of each distribution is consistent with the RV precision of each survey, and should not be interpreted as a resolved cluster velocity dispersion²⁵

We have RVs from Lick/Palomar (RV_{LP}) for nearly all stars listed in Table 6, except the 6 putative blue stragglers and 4 double-lined spectroscopic binaries (SB2s); and RVs from Hectochelle (RV_H) for 50 stars in the central square degree. The Hectochelle velocities are more precise (Figure 8), so whenever available, RV_H is used to determine the confidence in membership. Some stars have RV_{LP} within the highest confidence interval, and RV_H in a lower level. In these cases, if the star has ‘Y’ confidence level proper motions, RV_{LP} and photometry, we set the overall confidence to ‘P’, and consider the star a candidate SB1 (e.g. CWW 92 has $RV_{LP} = 45 \text{ km s}^{-1}$ and $RV_H = 25 \text{ km s}^{-1}$).

²⁵ M67, a much richer cluster, has a measured velocity dispersion of 0.5 km s^{-1} from radial velocities measured by Mathieu (1983). Assuming virial equilibrium, the cluster velocity dispersion can be approximated as $\sigma_v(\text{kms}^{-1}) \sim \sqrt{\frac{GM}{R}}$. With ~ 500 known members and similar size, we expect the M67 velocity dispersion to be about twice that of R147. If the 50 m s^{-1} RV precision estimate by Chubak et al. (2012) is valid, then the 0.5 km s^{-1} RV dispersion in our Keck RVs might actually be the intrinsic velocity dispersion for Ruprecht 147, on par with M67 despite the lower number of members.

3.3. The Color - Magnitude Diagram and Stellar Populations

Before assigning membership confidence designations, we check that the stars are confined to the region of color – magnitude space expected for a coeval stellar population with the properties we determine best describe R147.

We mapped out this locus by simulating a rich cluster with the properties we find for R147 from isochrone fitting (§4.4). Figure 9 shows CMDs for such simulated clusters. In this case, we simulated a cluster with 10^6 stars, with masses uniformly distributed between 0.6 and $1.6 M_{\odot}$. We set the binary fraction to 50%, with companion masses uniformly distributed between zero and the primary mass. Differential extinction is introduced according to a Gaussian with $\mu = 0.25$ and $\sigma = 0.05$ mag., and photometric precision is set at 0.02 mag. for $g'r'i'z'$ and 0.025 mag. for JHK_S . The simulated photometry is drawn from a Padova isochrone with $\log t = 9.4$ (2.5 Gyr), $[M/H] = +0.065$, and $m - M = 7.35$ mag. We bin, log-scale, and smooth the synthetic photometry to highlight the R147 locus in color – magnitude space.

Stars overlying the shaded region (basically, the region bound by the single star and equal mass binary sequences) are given the highest confidence designation. The simulation demonstrates that atypical differential reddening along a particular line of sight or relatively high photometric error can place stars outside the locus. Stars in these regions are assigned ‘P’. These could also be triple systems or exotic products of stellar mergers. CWW 67 is the only star existing beyond the equal mass triple sequence, and we assign it the lowest designation, ‘N’.

Confidence assignment is an iterative process, since we identify high-confidence members using isochrone fits, and these fits require a list of high-confidence members so that unlikely or non-members do not throw off the fit.

3.3.1. Stellar Populations

Blue Stragglers: In addition to the potential triple systems, 5 – 6 stars occupy a space of the CMD outside the cluster locus beyond the main sequence turnoff (MSTO): 6 clearly separate in the 2MASS CMD, but only 5 in $g'r'i'z'$. These five stars have proper motions consistent with the cluster, but lack RV measurements due to rotational line broadening (CWW 24, the sixth outlier in 2MASS, does have a measured $RV_{LP} = 41.8$ km s $^{-1}$, and so we assume that 2MASS photometric error is responsible for scattering it out of the cluster locus). We classify these 5 stars as blue stragglers (see Table 6, blue stragglers are listed as ‘BS’ in the Notes column). For the photometric probabilities, instead of the ‘Y/P/N’ scheme, we assign a ‘B’ for blue straggler.

Red Giants: We find 11 red giants in the cluster. The TERAPIX photometric errors suggest that only the four brightest red giants are saturated in $g'r'i'z'$ even with 1 second exposures. Other stars down to ≈ 9.5 are quoted as saturated in each band across the 4 fields. After consulting the raw frames, reduced images, and considering the 9.5 magnitude saturation limit found for other stars, we conclude that the entire red giant branch has unreliable optical photometry. This explains the apparent mismatch between our best isochrone fit and the optical

RGB.

CWW 14 is fainter and has reliable photometry, although it is 0.15 mag. blueward of the red giant branch in $(g' - i')$, and 0.08 mag. (4σ) blueward in $(J - K_S)$. Mathieu et al. (1990) identify a SB1 system in M67, S1040, which lies 0.2 mag. to the blue of the red giant branch in $(B - V)$. This system was previously suggested to consist of a star further down the giant branch with a companion star near the MSTO. Landsman et al. (1997) identified broad Lyman absorption features, demonstrating that the companion is actually a hot white dwarf, and that the system likely underwent a period of mass transfer. CWW 14 is an outlier in NIR, making it less likely to be a “red straggler”, and is probably a MSTO – RGB binary.

Main Sequence dwarfs: We use our best isochrone fit to determine approximate spectral types for the R147 membership. We assume masses of $1.1 M_{\odot}$ for G0 and $0.8 M_{\odot}$ for K0 dwarfs (Zombeck 2007), then locate the boundaries in the CMD from the isochrone. We find that the MSTO is located around mid-F. The subgiant branch down to F8 on the main sequence is well populated with ≈ 52 stars. We also identify ≈ 27 G dwarfs and ≈ 8 K dwarfs down to mid-K (We quote approximate numbers because of the approximate nature of our spectral typing). The 9 stars lacking $g'r'i'z'$ photometry appear in the 2MASS CMD as follows: 2 red giants, 3 MSTO F stars, 2 G dwarfs and 2 K dwarfs.

This method ignores the existence of binaries but illustrates the top-heavy nature of our membership list. This is likely due to a combination of observational bias and cluster evaporation (star clusters tend to lose their lowest mass members first, and ‘evaporate’ from the bottom up). The typical NOMAD proper motion error is ~ 10 mas/yr by $V \sim 12$. The K dwarfs have $V > 13$, making candidate identification from proper motions difficult. Therefore we are almost certainly missing significant numbers of low mass dwarfs.

3.4. Notes on Particular Stars

3.4.1. Apparent Non-members

CWW 77 has RVs inconsistent with R147 ($RV_{LP} = 51$ km s $^{-1}$, $RV_H = 52$ km s $^{-1}$), but its $(g' - i')$ and $(J - K_S)$ photometry place it near the equal mass binary sequence, so it could be an SB1.

CWW 67 has a low $RV_{LP} = 34$ km s $^{-1}$ and is 1.3 mag. above the $(g' - i')$ main sequence and 1.4 mag. above in $(J - K_S)$, but an equal mass triple would sit 1.2 mag. above the main sequence, so membership seems very unlikely (although a fourth lower mass companion could theoretically explain these discrepancies, so membership is difficult to definitively rule out).

CWW 72 sits ≈ 1 mag. above the main sequence in $(g' - i')$ and ≈ 0.75 mag. in $(J - K_S)$ – if a member, this could be a triple or an equal mass binary with inaccurate optical photometry. CWW 72 is a SB2, as seen in the Keck/HIRES spectrum. This star was observed previously at Lick and the spectrum exhibited no sign of binarity (otherwise we would not have selected it for observation with Keck). We also observed CWW 72 on two consecutive nights with MMT/Hectochelle. The CCF from the first night exhibits a tall and sharp peak with $RV_{H1} = 46.6$ km s $^{-1}$. The CCF from the second night is

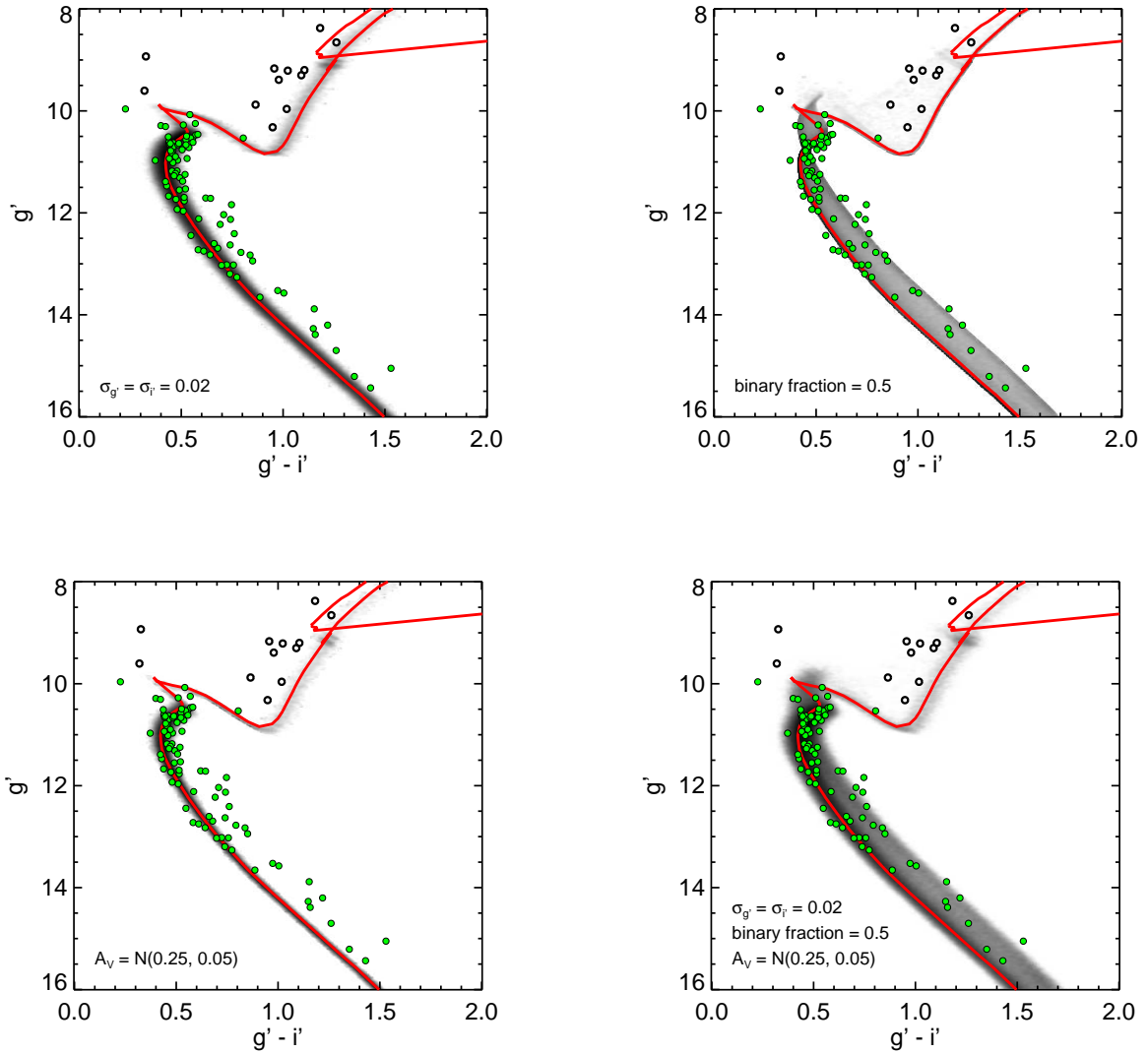


Figure 9. Each panel illustrates a source of main sequence broadening, demonstrating why the R147 main sequence might appear thicker than a textbook “beads on a wire” CMD. The R147 stars are plotted in green and saturated stars are plotted with an open circle. A Padova isochrone is overlaid in red with age = 2.51 Gyr, $m - M = 7.32$ ($d = 291$ pc), $A_V = 0.23$, and $[M/H] = +0.065$. The shaded regions in each panel represent simulations of 10^6 stars, with masses uniformly distributed between 0.06 and $1.6 M_\odot$, and photometry queried from the previously quoted Padova model. The simulated photometry has been binned (0.005 mag. in $g' - i'$, 0.01 mag. in g'), log scaled, and smoothed with a 5 pixel boxcar, to highlight possible regions of color-magnitude space occupied by R147 members. The top-left panel only includes photometric error, set at $\sigma_{g'i'} = 0.02$ and assuming normally distributed errors. The top-right panel only includes binaries, with the binary fraction set at 50%, and the secondary masses uniformly distributed between zero and the primary mass. The bottom-left panel only includes differential extinction, normally distributed about the typical cluster value of $A_V = 0.25$, with $\delta A_V = N(0, 0.05)$.

lopsided, suggesting that the signature of the companion was beginning to manifest and that the period of this system could be on the order of days. The CCF shape and resulting radial velocity from the first night point to a systematic velocity $\approx 5 \text{ km s}^{-1}$ greater than the R147 bulk motion, which cannot be explained by the cluster’s velocity dispersion or RV precision. If CWW 72 is a member, then it is (at least) a triple, perhaps with two approximately equal mass primary components orbiting with a period of days, and a fainter companion modulating the RV on a longer timescale (needed to explain the 5 km s^{-1} systematic offset).

Finally, CWW 50 sits 0.05 mag. blueward of the

$(g' - i')$ main sequence, but is on the $(J - K_S)$ main sequence. In Section 4.1 we discuss the possibility that this star is less extinguished and reddened than the rest of the cluster. If this is not the case, perhaps a hot white dwarf is pulling it blueward while not introducing much NIR flux, or there is an atypically large photometric error in one of the optical bands ($2\text{-}\sigma$), or else CWW 50 is not a member. We list it as ‘P’ because it is only inconsistent in $(g' - i')$, and while $RV_{LP} = 47.6 \text{ km s}^{-1}$, the Lick/Palomar velocity precision does not rule out membership.

3.4.2. Notes on 2MASS photometry

Table 2
Criteria for membership

Data	Source	Highest: Y	Probable: P	Low or Non-member: N
r_μ ^a	NOMAD, UCAC-3, Adam Kraus	< 5	5 – 8	> 8
Radial Velocity ^b	Lick & Palomar	39 – 47	36 – 39, 47 – 50	33 – 36, 50 – 53
Radial Velocity ($J - K_S$) CMD	Hectochelle 2MASS	40 – 43 Overlaps with simulation ^c	38.5 – 40, 43 – 44.5 ± 0.2 mag.	else beyond equal mass triples
($g' - i'$) CMD	CFHT/MegaCam	Overlaps with simulation	± 0.2 mag.	beyond equal mass triples

Note. — See Section 4 for a discussion of membership criteria. Values in parenthesis denote acceptable ranges. Values equal to endpoints are assigned to the higher level

^a Radial distance in proper motion space from the mean value for R147, with units of mas/yr.

^b Radial velocities measured in km s⁻¹.

^c See Section 3.3 and/or Figure 9 for discussion

Our $g'r'i'z'$ imaging shows CWW 51 is an optical double, with a star 1.65 arcseconds away with a similar $g'r'i'z'$ SED (the magnitude difference in each band is 0.02 – 0.05 mag. between the two stars). The components are separated by 1.65", which translates into a minimum physical separation of 495 AU, assuming a cluster distance of 300 pc. This suggests that the pair actually form a wide binary, although their angular proximity could also be explained by a chance alignment. This double was not resolved in the 2MASS Point Source Catalog. Adding 0.75 mag. to the J band magnitude (halving the brightness, to reflect just the one star) moves CWW 51 next to the stars it neighbors in the ($g' - i'$) CMD. Table 6 quotes, and the figures in this work plot, the 2MASS photometry for CWW 51, despite this realization, although we do include a footnote referencing this in the Table.

The 2MASS Point Source Catalog provides PSF photometry by default in most cases. Figure 10 shows 23 outlier stars on either side of the ($J - K_S$) main sequence, out of the 80 stars ‘Y/P’ stars with aperture photometry that are not blue stragglers. If aperture photometry is used instead, each of these stars moves towards the cluster locus. No star already in the locus shifts appreciably outside when aperture photometry is used instead. One star slides from blueward from the main sequence by 0.037 mag., or approximately equal to the J and K_S errors added in quadrature. The fact that the majority of outliers’ photometry systematically moves toward the cluster locus suggests to us that for many stars in these fields and at these magnitudes, the aperture photometry is superior. We do not assign lower confidence levels to PSF photometry outliers, if their aperture photometry is consistent with membership. We include the aperture photometry for 18 stars in Table 6 and all other figures (CWW 22, 24, 27, 28, 30, 37, 38, 43, 48, 49, 57, 59, 67, 68, 90, 91, 94, and 100).

3.4.3. SB2 systems

CWW 64, 65, 66, 68, and 72 showed double-peaked cross-correlation functions in one of the RV epochs, indicating these systems to be nearly equal mass binaries (the case of CWW 72 is discussed above). Figure 11 plots the ($g' - i'$) and ($J - K_S$) CMDs, with the five SB2s highlighted red. The single star and equal mass binary sequences from our best isochrone fit (Padova model) are plotted in green. All five SB2s are clustered around the equal mass binary sequence, corroborating their equal

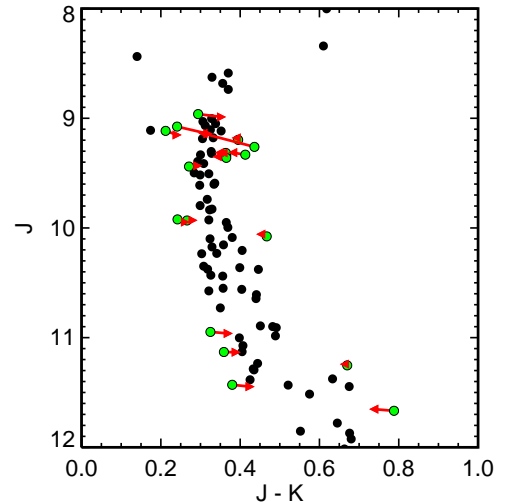


Figure 10. PSF photometry (green circles) vs aperture photometry (red triangles) for 18 outliers on the 2MASS ($J - K_S$) CMD. All shift closer to the locus when the aperture photometry is used instead of the default PSF photometry. No star already in the locus shifts appreciably outside when aperture photometry is used instead. One star slides from blueward from the main sequence by 0.037 mag., or approximately equal to the J and K_S errors added in quadrature (not shown).

mass status and the validity of our isochrone fit.²⁶

3.4.4. SB1 binary candidates from discrepant RVs

Figure 11 also plots in cyan 10 stars with Hectochelle RVs inconsistent with the cluster: CWW 19, 22, 27, 53, 69, 70, 77, 92, 95, 99, and 106 (CWW 19 is a red giant. We do not include it in the optical plot because it is saturated). In Section 3.2 we suggested CWW 92 is a SB1 from the 20 km s⁻¹ difference between RV epochs. All other SB1 candidates have similar RVs from Lick/Palomar and Hectochelle, and are considered candidate SB1s because RV_H is at least a few standard deviations away from the cluster average, although this discrepancy forces a ‘P’ classification (except CWW 77, which we classify as ‘N’ as noted above).

²⁶ CWW 68 actually sits on the equal mass triple sequence. Both CWW 64 and 65 are midway between the equal mass binary (-0.75 mag.) and triple (-1.2 mag.) sequences, at 1.0 mag. brighter than the main sequence, which can occur when an equal mass binary system, which manifests as the SB2, has a third companion with 50% the luminosity of each primary.

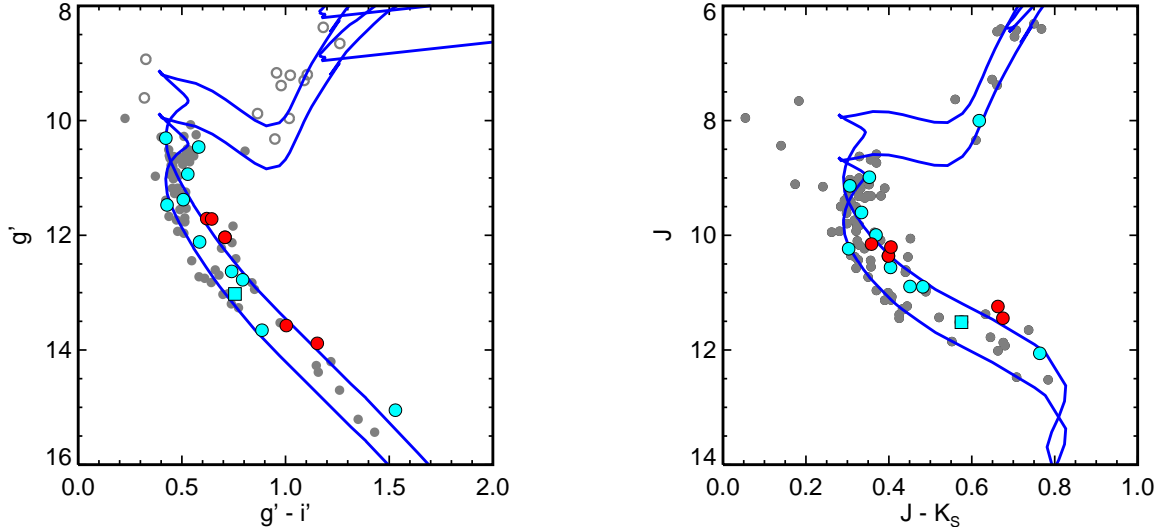


Figure 11. Ten stars with discrepant Hectochelle RVs are plotted in cyan (RV more than 1.5 km s^{-1} away from cluster average). Five SB2s are plotted in red. The rest of the cluster is shown in gray, with our best fit isochrone (Padova model) overplotted in dark blue showing the single and binary sequences ($\log t = 9.4$, $[M/H] = +0.064$, $m - M = 7.32$, $A_V = 0.23$). All of the SB2s were identified by a double-peaked cross-correlation function, which indicates these should be nearly equal mass ratio systems. The fact that they are all clustered around the binary sequence (shifted “up” 0.75 mag.) corroborates their equal mass status and the validity of our isochrone fit. All but 3 SB1 candidates are also shown near or on the binary sequence. The square shows CWW 99 on the $(g' - i')$ single star sequence, but in $(J - K_S)$ the star is 0.5 mag above this sequence. The other two stars might be high-mass ratio systems (and therefore do not manifest in shifts on the CMD), stars that have received gravitational kicks (so their RVs are no longer consistent with the cluster), or are non-members.

Figure 11 shows all but CWW 70 are clustered around the binary sequence. CWW 70 has $RV_{LP} = 38 \text{ km s}^{-1}$ and $RV_H = 39 \text{ km s}^{-1}$. Despite this $2\text{-}\sigma$ discrepancy, we cannot rule out membership. The star might have a low mass companion or received a gravitational “kick”. For example, a G2 V ($1 M_\odot$) – M0 V ($0.5 M_\odot$) binary system with semi-amplitude velocity $K_1 = 5 \text{ km s}^{-1}$, zero eccentricity and zero inclination, will have a period $P \approx 12$ years. The large luminosity difference in a high mass ratio binary means the system will not stand out in either photometry (it will lie on the single star sequence) or in spectra (the secondary is too faint to manifest as a SB2). This means although the RVs for CWW 70 are inconsistent with single star membership, we cannot rule out the possibility of a low mass companion at large separation, which would induce a measureable velocity offset, but modulated at a period much longer than our 2 year baseline.

CWW 99 is plotted as a blue square in Figure 11. It sits on the single star $(g' - i')$ sequence, but is 0.5 mag above the $(J - K_S)$ sequence. This can be explained by a low mass companion, which would show up more prominently in NIR than optical.

4. INFERRING CLUSTER PROPERTIES

The properties of stellar clusters (age, composition, distance and interstellar extinction) are commonly estimated by fitting isochrones to broadband photometric color – magnitude diagrams (CMD). Often a “chibi-eye” technique is employed, where sets of isochrones representing varying cluster parameters are overlaid on a CMD, and the apparent best fit or series of best fits are selected to establish acceptable ranges for these fundamental parameters. This technique can be successful

when one or more of these properties can be well constrained. For example, clusters might be nearby or sit above/below the galactic plane and suffer little extinction, and the closest benchmarks have parallax distances from Hipparcos and/or HST/FGS. These independent constraints break the high degree of degeneracy between each variable (e.g. metallicity works in a similar direction to the interstellar reddening vector).

None of Ruprecht 147’s properties have been previously well measured. At a distance of over 200 pc, the cluster has a HIP2 distance measurement from 3 stars that appears unreliable and is apparently too close by a significant fraction (§4.7). We first describe our efforts to independently constrain the interstellar extinction with the Schlegel et al. (1998) dust map (§4.1), and the composition from spectroscopic analysis (§4.2), then we will use isochrone models to determine the cluster’s age and distance. Specifically, we fit a spectroscopically derived $T_{\text{eff}} - \log g$ diagram with Padova isochrones with abundances fixed by the spectroscopic metallicity (§4.3). We then query the resulting best fit Padova isochrone for a star with T_{eff} and $\log g$ closest to the values for the early G dwarf we derive with SME, and perform a brute force χ^2 SED fit for distance and visual extinction to the resulting synthetic $g'r'i'JHK_S$ photometry.

Next we develop an efficient and automated 2D cross-correlation isochrone fitting technique, and fit Padova and Dartmouth models to the $(g' - i')$ and $(J - K_S)$ CMDs to determine the age, distance and visual extinction. We will see that the NIR and optical fits agree very well with each other (Figures 17, 18). We also fit the $(g' - i')$ CMD with the τ^2 maximum-likelihood method, and derive consistent results, validating our isochrone fitting technique. We find an age from both NIR and

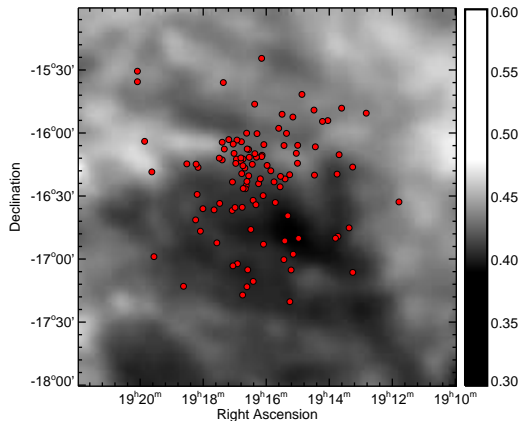


Figure 12. Visual extinction map with R147 members designated by red dots. A_V calculated from the dust map of Schlegel et al. (1998), assuming $R_V = 3.1$. The map was smoothed with a 3 arcminute boxcar.

optical photometric isochrone fitting consistent with our spectroscopic results, which supports our earlier decision to break the degeneracy between these parameters with this age (§4.4).

We will compare results from Padova, Dartmouth and PARSEC models; and then discuss the differences between our photometric distance and the parallax distance inferred from 3 HIP2 cluster members. Finally, we synthesize the results from these various isochrone fits and present our preferred set of parameters describing the age, composition, distance and visual extinction for Ruprecht 147 (§5).

4.1. Interstellar Extinction

The large apparent size of R147 on the sky introduces the possibility of differential extinction across the cluster. Figure 12 plots A_V from the dust map of Schlegel et al. (1998), assuming $R_V = 3.1$ ²⁷. Many cloud structures are apparent in the field, showing A_V to vary from 0.3 – 0.5 mag.

Considering the cluster’s proximity, some of this dust undoubtedly lies beyond the cluster. Drimmel & Spergel (2001) determine the Sun to lie 14.6 ± 2.3 pc above the Galactic midplane, and measure a dust scale height of $h_d = 188$ pc at the Solar Circle. The Galactic latitude of R147 ranges from -12° to -14° . At a distance of 250 – 300 pc, this latitude places R147 50 – 70 pc below the Sun, and 35 – 55 pc below the midplane (less, if a larger Z_\odot is assumed), or about 20-30% of the dust scale height. The local bubble has very little dust in it out to ~ 150

²⁷ Many studies have demonstrated that on average, $R_V = 3.1$ for a diffuse ISM. This relationship between extinction and reddening is of course dependent on the composition and physical conditions in the intervening ISM. Considering Ruprecht 147, there are no dense molecular clouds along the line of sight. We also do not expect any additional reddening intrinsic to the cluster or its stars, because this is an old cluster, and it and its stars are no longer enshrouded in dust and gas. Recently, Jones et al. (2011) used over 56,000 Sloan M dwarf spectra to map visual extinction and R_V in the nearby Galaxy. While their R_V distribution peaks near 3.1, their median value is actually 3.38, and ranges from 2 to 5.5. We will assume the canonical value of $R_V = 3.1$ for the diffuse ISM for this preliminary study and intend to return to this issue in a future work.

pc (Lallement et al. 2003), suggesting it is possible that most of the dust is behind the cluster.

Section 3.3 described star cluster simulations used to assess photometric membership probabilities, by introducing photometric scattering sources to explain the observed width of the R147 main sequence, including photometric error, binarity, and differential extinction. Figure 9 plots simulated cluster CMDs including each of these photometric scattering sources separately, and all combined. The binarity simulation demonstrates that the single star and equal mass binary sequences pinch together near the MSTO. Differential reddening smears the CMD along a negative-sloped diagonal (extinction plus reddening). If there is non-negligible differential reddening, the “binary pinch” should be smeared out.

Unfortunately, we have only identified 6 members at this pinch. Figure 13 shows four are confined within the pinch. CWW 50 sits 0.08 mag. blueward, and CWW 53 sits 0.06 mag. redward. These values are 2 – 3 times larger than the expected photometric error. CWW 53 has RVs from two epochs at 5 km s^{-1} greater than the cluster mean, and photometry placing it near the equal mass triple sequence. The uncertainty in membership and multiplicity means we cannot use CWW 53 to test for differential reddening. CWW 50 must be reddened by $\delta A_V = 0.13$ mag. in order to place it on the single star sequence. In Section 4.3, we find an optimal $A_V = 0.23$ mag., so a particular line of sight of $A_V = 0.10$ mag. is not impossible. Ideally, we would like to check if the nearest R147 neighbors to CWW 50 also appear less extinguished than expected. Unfortunately, the nearest neighbor is $\sim 10'$ away. It is also noteworthy that the Schlegel et al. (1998) dust map extinction along this line of sight is $A_V = 0.296$ mag., the lowest value in the entire field, and 0.13 mag. lower than the median A_V for the region of radius $r = 1^\circ.2$ encompassing all R147 members.

The R147 main sequence is thicker than 1 magnitude at various points. Unfortunately in many cases, our radial velocities do not have sufficient precision to firmly establish these stars as cluster members (we still designate them ‘Y’ members because the RVs are consistent with the R147 bulk motion, within the precision of our Lick/Palomar RV survey). We also only have one RV epoch for the majority of stars, and so stellar multiplicity is impossible to diagnose at this point. More precise velocities are required before we attribute these photometric outliers to differential extinction.

There is also a strip of 7 main sequence dwarf stars blueward of our best isochrone fit in the $(g' - i')$ CMD. Adding $\delta A_V = 0.05$ mag. to these stars shifts them onto the isochrone. This translates into a 0.03 mag. shift in color, which is within the photometric precision, and so differential extinction is not required to explain these stars apparent blueward offset in the optical CMD. No net offset is seen in the NIR CMD.

We will postpone further investigation into differential extinction to a future study, and in this work will fit single A_V models, with values constrained by the dust map at $A_V < 0.5$.

4.2. Metallicity

We analyzed five Keck/HIRES spectra with Spectroscopy Made Easy (SME, Valenti & Piskunov 1996), using the procedure described in Valenti & Fischer

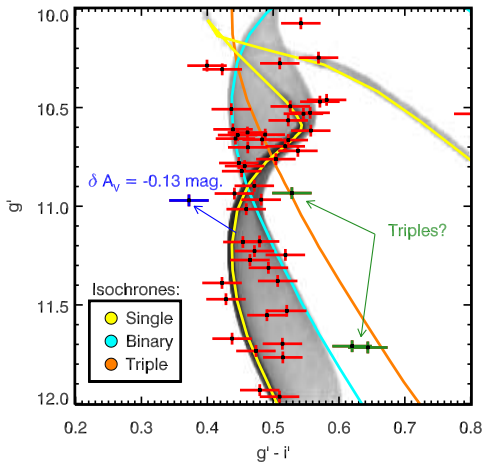


Figure 13. Looking for differential extinction. The ‘Y’ and ‘P’ members are plotted with 0.03 mag. error bars in color and magnitude. Single star (yellow) and equal mass binary (cyan) sequence isochrones (Padova) are plotted with $\log t = 9.4$, $[M/H] = +0.1$, $m - M = 7.48$, and $A_V = 0.23$. The gray shading illustrates the results of our Monte Carlo cluster simulation, including binaries and neglecting differential extinction and photometric error, from Figure 9 (top – right panel). The single and binary sequences cross at $g' \approx 10.9$, forming a “pinch” at the turnoff. Differential extinction should smear this pinch along the reddening vector shown in blue. The three outliers redward of the binary sequence could be triples. CWW 50, the one outlier blueward of the single star main sequence, might either suffer atypically large photometric error, or is not a member, or else needs to be reddened by $\delta A_V = 0.13$ in order to place it on the main sequence. Interestingly, the visual extinction from the Schlegel et al. (1998) dust map at the position of CWW 50 is the lowest in the field, and exactly 0.13 mag. lower than the median value for the region of radius $r = 1^\circ.2$ centered on the cluster and encompassing all R147 members.

(2005). SME uses the Levenberg-Marquardt algorithm to fit observed echelle spectra with synthetic spectra generated assuming LTE and plane-parallel geometry, yielding effective temperature, surface gravity, metallicity, projected rotational velocity, and abundances of the elements Na, Si, Ti, Fe, and Ni²⁸

Upon obtaining an initial fit to a spectrum, T_{eff} was perturbed $\pm 100\text{K}$ and run again. The three solutions were then averaged, with the standard deviation set as the parameter uncertainty, except in cases where this uncertainty is less than the statistical uncertainties measured in Valenti & Fischer (2005): 44 K in effective temperature, 0.03 dex in metallicity, 0.06 dex in the logarithm of gravity, and 0.5 km s^{-1} in projected rotational velocity. Additional corrections are applied to the final values based on the analysis in Valenti & Fischer (2005) of Vesta and abundance trends in binary pairs with T_{eff} (see Figure 14 for the CWW 44 Keck/HIRES spectrum

²⁸ Valenti & Fischer (2005) did not solve for magnesium abundance because of the degeneracy between $[Mg/Fe]$ and $\log g$ when fitting the synthetic spectra to the gravity-sensitive Mg b triplet (Thackeray 1939). Fuhrmann et al. (1997) recommends fitting for $[Mg/Fe]$ first, using the weak Mg i lines at $\lambda 4571$ or $\lambda 5711$, and then fixing the abundance and fitting the Mg b wings to derive $\log g$. Valenti & Fischer (2005) decided to exclude from analysis wavelengths $\lambda < 6000 \text{ \AA}$, except for the region encompassing the Mg b triplet, because of severe line blending in the blue in cool stars which would complicate the spectral synthesis fit.

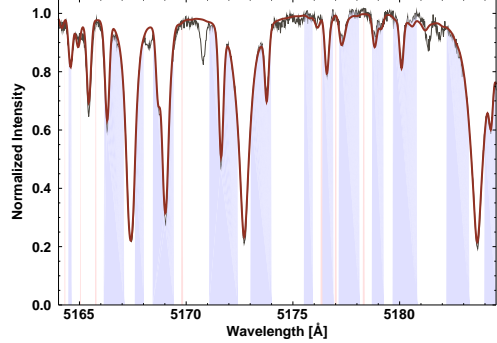


Figure 14. A Keck/HIRES spectrum of the order encompassing the Mg b triplet for CWW 44, an F MSTO star, is shown in black. The synthetic spectrum resulting from our SME analysis is overlaid in red. The spectrum segments included in the fit are highlighted in purple, and the salmon stripes identify the continuum regions. Table 3 lists our SME results for this and four other stars.

and SME synthetic spectrum fit in the order encompassing Mg b).

Our results for the five stars are presented in Table 3 and indicate that the cluster has a slightly super-Solar metallicity of $[M/H] = +0.07 \pm 0.03$, from CWW 91, 44 and 21²⁹. We neglected the results from CWW 22 because it is hottest (complicating the fit to gravity, described in the next subsection) and has the poorest χ^2_ν fit. Valenti & Fischer (2005) suggest using $[Si/H]$ as a proxy for the α -process abundance. We find $[\alpha/Fe] = [Si/H] - [Fe/H] \approx 0.0$ ($[Si/Fe] = -0.03$ and 0.0 for CWW 44 and 91).

We find a much lower metallicity for CWW 78, $[M/H] = -0.11 \pm 0.03$ and $[Fe/H] = 0.0 \pm 0.02$. This outlier has otherwise satisfied every criterion for membership, with proper motions, photometry and a precise RV all consistent with the cluster. For this work, we will assume that this peculiar metallicity can be explained by a complication in the SME analysis, and will look into this in a future study.

Pakhomov et al. (2009) analyzed high-resolution, high signal-to-noise spectra of three red giant members of R147, and their results are compiled in Table 3. The first star, HD 179691, has a radial velocity inconsistent with the cluster, indicating it is either an SB1 or not a member. The other two red giants show super-Solar iron abundance, consistent with our SME results.

In the future, we will more rigorously determine the cluster metallicity combining photometry, spectroscopy, and cluster properties.

4.3. Fitting Isochrone Models to Spectroscopic Properties

Figure 15 shows the $T_{\text{eff}} - \log g$ diagram resulting from our SME analysis, along with a $(g' - i')$ CMD for the 5 stars, along with their CWW IDs. The CMD shows that our SME results place the stars on the $T_{\text{eff}} - \log g$ diagram with the correct relative positions. We have selected

²⁹ We will often use $[M/H] = +0.064$ throughout this work, because of the way the Padova isochrone webtool parameterizes metallicity: $[M/H] = \log(Z/Z_\odot)$, with $Z = 0.019$. Setting $Z = 0.022$ gives $[M/H] \approx +0.064$.

Table 3
Spectroscopic analysis of R147 stars

Property	CWW 44 ^a	CWW 91 ^a	CWW 21 ^a	CWW 22 ^a	CWW 78 ^a	HD 179691 ^b	HD 180112 ^b	HD 180795 ^b
Type	mid-F MSTO	G0/2 V	subgiant	mid-F MSTO / SB1?	late-F V	K1 III	K0 III	K0 III
T_{eff} (K)	6273 (5)	5747 (62)	6129 (25)	6350 (80)	6115 (52)	4573 (80)	4733 (80)	4658 (80)
$\log g$ (gm cm s ⁻²)	4.11 (0.02)	4.35 (0.11)	3.79 (0.07)	3.6 (0.06)	4.27 (0.08)	2.28 (0.15)	2.53 (0.15)	2.43 (0.15)
RV (km s ⁻¹)	41.41	41.50	40.35	46.63	41.02	46.7	40.1	40.8
$v \sin i$ (km s ⁻¹)	6.87 (0.69)	0.32 (0.33)	6.50 (0.61)	6.91 (0.73)	6.09 (0.65)	-	-	-
[M/H]	0.07 (0.01)	0.06 (0.03)	0.09 (0.03)	-0.01 (0.04)	-0.11 (0.03)	-	-	-
[Na/H]	0.22 (0.02)	0.23 (0.01)	0.12 (0.01)	-0.02 (0.08)	-0.14 (0.03)	0.24	0.16	0.24
[Si/H]	0.14 (0.01)	0.11 (0.02)	0.10 (0.01)	0.00 (0.03)	0.02 (0.02)	0.08 ± 0.08	0.15 ± 0.06	0.25 ± 0.08
[Ti/H]	0.28 (0.02)	0.16 (0.02)	0.25 (0.03)	0.03 (0.05)	0.06 (0.04)	-0.03 ± 0.07	0.04 ± 0.05	-0.02 ± 0.04
[Fe/H]	0.17 (0.01)	0.11 (0.02)	0.22 (0.01)	0.08 (0.03)	-0.00 (0.02)	-	-	-
[FeI/H]	-	-	-	-	-	0.03 ± 0.06	0.14 ± 0.06	0.16 ± 0.04
[FeII/H]	-	-	-	-	-	-0.02 ± 0.09	0.07 ± 0.07	0.08 ± 0.04
[Ni/H]	0.07 (0.01)	0.05 (0.02)	0.13 (0.01)	-0.03 (0.06)	-0.02 (0.03)	-0.04 ± 0.08	0.04 ± 0.06	0.12 ± 0.07
χ^2_{ν}	2.90	2.86	4.07	5.88	2.18	-	-	-
$\log t$ (years)	-	-	-	-	-	9.2 ± 0.5	9.0 ± 0.4	9.0 ± 0.4

Note. — Rows and SME statistical uncertainties: (Type) Rough Spectral Type, (T_{eff}) Effective Temperature: $\sigma = 44$ K, ($\log g$) Surface Gravity: $\sigma = 0.06$ dex, (RV) Radial Velocity ($v \sin i$) projected rotational velocity: $\sigma = 0.5$ km s⁻¹, ([M/H]) Metallicity = $\log_{10} Z/Z_{\odot}$ ([Na/H] .. [Ni/H]) Sodium, Silicon, Titanium, Iron and Nickel abundance: $\sigma = 0.03$ dex, (χ^2_{ν}) Reduced χ^2 of the fit, ($\log t$) age in years assuming $d = 280$ pc

^a Our SME analysis results of Keck/HIRES spectra

^b Red giants analyzed by Pakhomov et al. (2009), reproduced here for comparison.

Padova isochrone models with $[\alpha/\text{Fe}] = 0$ and $[\text{M}/\text{H}] = +0.1$, and attempt a “chi-by-eye” fit by overlaying models with ages at $\sim 2, 2.5$, and 3 Gyr ($\log t = 9.3, 9.4, 9.5$). Fitting the $T_{\text{eff}} - \log g$ diagram is powerful because it is independent of $m - M, A_V$, and color - temperature transformations.

The MSTO star CWW 44 in theory provides a tight constraint on age and metallicity, but we are cautious of the accuracy of $\log g$, because the broad wings of the Mg b lines provide the gravity constraint, and their sensitivity decreases at higher temperature and lower gravity. Jeff Valenti has suggested that the Mg b wings provide useful constraints on gravity for dwarfs cooler than ~ 6200 K³⁰, which is approximately the temperature for 4 of 5 stars we analyze. Fuhrmann et al. (1997) is able to derive an accurate $\log g$ for Procyon (F5V) from Mg b, so perhaps our concern is unwarranted. Assuming we have derived accurate stellar properties, we find that models fit best with $\log t = 9.4 \pm 0.05$ (2.25 - 2.8 Gyr), which encompass the error bars of CWW 44.

The models barely pass through the error bars for the early G dwarf, CWW 91, even though this should be the one star of the five we know has broad enough Mg b wings to provide adequate constraint on $\log g$, since it is most similar to the Sun. If we fix $\log g$ according to the Padova isochrone ($\log t = 9.4$ (2.5 Gyr) and $[\text{M}/\text{H}] = +0.064$), we find $\log g = 4.45$ instead of 4.35, at mass $M = 1.03 M_{\odot}$.

We queried the $g'r'i'$ and JHK_S photometry for a $1.03 M_{\odot}$ star from this isochrone and perform a brute force least-squares fit for distance modulus and visual extinction for CWW 91 in the range $m - M = 7 - 8$ and $A_V = 0 - 0.5$, with 0.01 mag. step sizes, JHK_S errors according to 2MASS ($\sigma = 0.023, 0.026, 0.021$ mag.) and $g'r'i'$ errors set to $\sigma = 0.03$ mag. We find a minimum χ^2 at $m - M = 7.44 \pm 0.02, A_V = 0.25 \pm 0.03$. (see Figures 15, 16). We perturbed $[\text{M}/\text{H}] \pm 0.02$ dex (our error bar from the SME analysis) and $\log t \pm 0.5$ (our error bar from fitting isochrones to the $T_{\text{eff}} - \log g$ diagram), then re-fit and find uncertainties of 0.04 and 0.01 mag. for $m - M$ and A_V . We then perturbed T_{eff} by ± 50 K (the SME statistical error bar) and re-fit, and find uncertainties of 0.06 and 0.04 mag. for each parameter.

Adopting these conservative errors, we find $m - M = 7.44 \pm 0.06$ and $A_V = 0.25 \pm 0.04$. We repeated this analysis with solely the optical $g'r'i'$ photometry, and then with just the 2MASS NIR JHK_S photometry, and find $m - M = 7.44$ and 7.41 respectively, and $A_V = 0.18$ for both cases. This give us confidence in the $g' > 10$ CFHT photometry.

We introduced reddening to the synthetic SED using the relationships provided by the Padova CMD website³¹: $A_{g'}/A_V = 1.167, A_{r'}/A_V = 0.860, A_{i'}/A_V = 0.656, A_J/A_V = 0.290, A_H/A_V = 0.183, A_{K_S}/A_V = 0.118$.

4.4. Fitting isochrone models to broadband photometry

Up to this point, we have fit isochrones to a $T_{\text{eff}} - \log g$ diagram with values derived with SME for 5 stars with Keck/HIRES spectra. Now we perform a more tra-

ditional fit to the broadband optical and NIR photometry of all cluster members, and find results consistent with our spectroscopic solution. We initially worked with Padova models (Girardi et al. 2000; Marigo et al. 2008)³² because they were the only group, to our knowledge, that provided isochrones in the CFHT/MegaCam $g'r'i'z'$ filter set. Aaron Dotter has since released Dartmouth models in this set, and we will briefly compare results between these two models in Section 4.6.

Given the high degree of degeneracy between age, distance and visual extinction (we fix metallicity according to our SME result, $[\text{M}/\text{H}] = +0.064, [\text{Fe}/\text{H}] = +0.1$), we developed an automated isochrone fitting technique that can efficiently cover a large parameter space. Inspired by the τ^2 method of Naylor & Jeffries (2006), described and utilized in Section 4.5, our method simulates a star cluster with a particular age and composition, and computes 2D cross-correlations between the resulting synthetic and actual CMD density distributions in order to find the distance and visual extinction that best aligns the model to the data. The age and composition control the morphology of the stellar locus on a CMD, while changes in distance modulus and extinction simply translate the locus across the CMD plane.

Using our cluster simulator (§3.3), we map the stellar locus with 10^4 stars, the binary fraction set at 70%, and no differential extinction, for ages ranging from 1 to 4 Gyr. The simulated cluster CMD is binned by 0.005 magnitudes in each dimension, as is the actual R147 CMD. Photometric error is not introduced to the synthetic photometry. Instead, the position for each star on the real CMD is broadened by a 2D gaussian according to the assumed photometric error for each band: we use 0.02 mag. for g' and i' , and the errors provided by the 2MASS Point Source Catalog for J and K_S .

For the NIR ($J - K_S$) fit, all ‘Y’ members were binned except for the blue stragglers, and the giants that appear to be undergoing core helium fusion according to their optical and NIR photometry offset from the main red giant branch. Dotter et al. (2008) note that the Padova isochrones are hotter in the lower main sequence, starting at $\approx 0.8 M_{\odot}$, than other commonly used models including the DSEP (Dartmouth Stellar Evolution Program) and Yale-Yonsei (Y²). The left and central panels of Figure 20 illustrates this difference in $T_{\text{eff}} - \log g$ and ($g' - i'$), but the right panel shows that the discrepancy does not significantly affect the NIR isochrone. We do remove the K dwarfs from our optical isochrone fits. We also discard the optical red giant branch because of the saturated i' band photometry.

We compute the 2D cross-correlation between the real and synthetic CMD distributions with the IDL function CONVOLVE. Locations on the resulting image corresponding to negative extinction are set to zero. The point of peak signal provides the shift required to best align the isochrone model to the data.

Although this is not a statistically rigorous method for isochrone fitting, this cross-correlation method is conceptually straightforward, simple to code, it can efficiently test hundreds of models in an automated fashion to more quickly cover the age - composition parameter space (a

³⁰ <http://www-int.stsci.edu/~valenti/sme.html>

³¹ for a G2 dwarf, using a Cardelli et al. (1989) extinction curve with $R_V = 3.1$

³² <http://stev.oapd.inaf.it/cgi-bin/cmd>

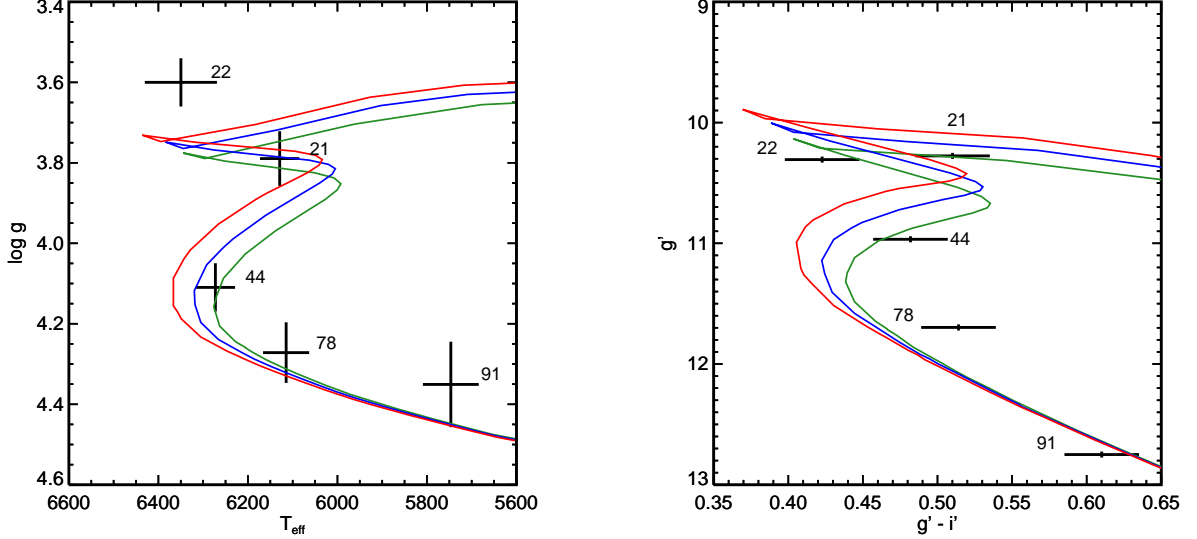


Figure 15. Left: $T_{\text{eff}} - \log g$ diagram of five stars with Keck/HIRES spectra and properties derived with SME. Numbers indicate CWW ID. Padova isochrones overlaid with $[M/H] = +0.064$ and $\log t = 9.3$ (blue, 2 Gyr), 9.4 (red, 2.51 Gyr), and 9.5 (green, 3.16 Gyr). Isochrones with ages of 2.34 and 2.7 Gyr encompass the error bars of CWW 44. The red isochrone at 2.51 Gyr shows the best fit to these spectroscopic properties; we also derive this age solution in our isochrone fits to NIR and optical photometric color-magnitude diagrams. Right: CFHT/MegaCam ($g' - i'$) CMD for the same five stars, with 0.03 mag. error bars. Padova isochrones of same age and color scheme are overlaid with $m - M = 7.35$, $A_V = 0.25$. For a discussion, see §4.3.

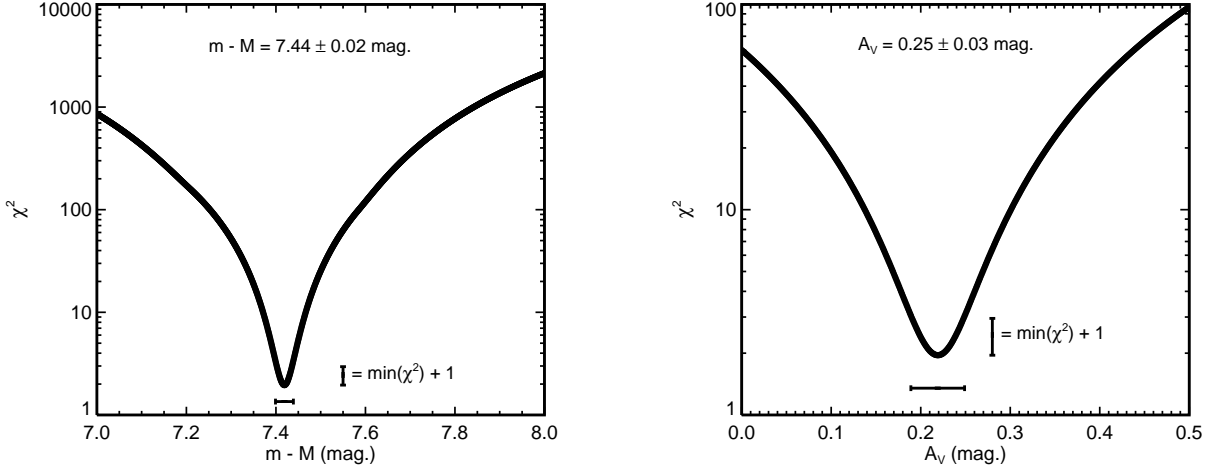


Figure 16. Inferring distance and extinction: brute force least squares fit of $g'r'i'JHK_S$ photometry for CWW 91 to a $1.03 M_{\odot}$ star with SED drawn from a Padova isochrone with $\log t = 9.4$ and $[M/H] = +0.064$ (mass, age and metallicity suggested by SME analysis of a Keck/HIRES spectrum). We calculate $\chi^2 = \Sigma (x_i - \mu_i)^2 / \sigma_i^2$, where x_i is the measurement, μ_i is the model value, and assuming $\sigma_{g'r'i'} = 0.03$ mag. and $\sigma_{JHK_S} = 0.025$ mag. χ^2 is minimized at $m - M = 7.44 \pm 0.02$ and $A_V = 0.25 \pm 0.03$. See §4.3 for a discussion.

few minutes), and it provides a diagnostic for model selection: the model with the maximum cross-correlation signal. In the next section, we will demonstrate that this method provides solutions essentially identical to the τ^2 maximum likelihood method. Three panels in Figure 17 plot age, distance and extinction versus the cross-correlation signal, normalized to the maximum value, with metallicity fixed at $[M/H] = +0.064$. The results from fitting Dartmouth models are also plotted, and offset by +0.06 for clarity: see §4.6. Although broad, there are clear peaks in each diagram at $\log t = 9.4$ (2.51 Gyr), $m - M = 7.32$ (291 pc), and $A_V = 0.23$

or $E(B - V) = 0.075$ assuming $R_V = 3.1$.

The fourth panel of Figure 17 plots the isochrones (gray) of each solution for $\log t = 9.1$ to 9.56, in steps of 0.01. The R147 members used in the fit are plotted in black. The best model quoted above is overlaid in yellow, and two additional models are also included at younger and older ages, providing points of reference for how the fits appear to rotate across the CMD counter clockwise with increasing age. This rotation is primarily caused by the overabundance of cluster members at the MSTO, which serves to anchor each fit to the MSTO location. Those models which also pass through the handful of K

dwarfs and red giant branch are rewarded with a higher cross-correlation signal, creating the broad peaks in the other panels of Figure 17. Perhaps if the K dwarfs and red giants were weighted more heavily than the turnoff stars we would see more strongly peaked results.

We ran the optical fit with $[M/H] = +0.08$ and find the best model is $\log t = 9.39$, $m - M = 7.35$, $A_V = 0.26$. The optical results are presented in Figure 18. The consistency between the optical and NIR CMD fits and the parameters obtained with the $T_{\text{eff}} - \log g$ diagram further justifies our use of these preliminary optical data.

4.5. Validating our method with τ^2

Naylor & Jeffries (2006) have developed a maximum-likelihood method called τ^2 for fitting model isochrones to color – magnitude diagrams (see also Naylor 2009)³³. This method simulates a cluster CMD from an isochrone, with a user-defined binary fraction. The user supplies a star catalog including the color, magnitude, and photometric errors which the τ^2 code assumes are normally distributed. This method is powerful because it naturally accommodates errors in both color and magnitude, and accounts for the binary sequence. The code performs a grid search across a specified range of distances and ages, for isochrones of a given metallicity and reddening, and identifies best values, confidence intervals, and returns two diagnostics for assessing how well the model describes the data: a reduced- τ^2 (analogous to χ^2_ν) and a probability value, Pr .

While the τ^2 code includes an isochrone library, we make use of the user-supplied isochrone feature and pass it the Padova grids, with $[M/H] = +0.064$. The τ^2 code does not currently solve for A_V , so we de-redden our catalog before running τ^2 , and iterate for a range of reddening values. We selected the 56 R147 members of highest confidence (‘Y’), excluding the later K dwarfs and red giants. We ran τ^2 for $A_V = 0.0$ to 0.5, and allowed τ^2 to search distances ranging from 200 to 400 pc (range suggested by the HIP1 (~ 270 pc) and HIP2 (~ 200 pc) parallaxes, plus a little extra on the far side), and ages 1 to 4 Gyr (step size is 0.01 in $\log t$, encompassing the 2.5 Gyr value suggested by our fit to the $T_{\text{eff}} - \log g$ diagram in Figure 15).

We find high probabilities for a large suite of models demonstrating the flatness of the τ^2 space and high degree of degeneracy between age, metallicity, distance and extinction. The degeneracy is accentuated in this particular case because we had to remove the saturated red giant branch from the fit. Figure 19 plots the best distance and age values for the range of extinctions. If we apply the age constraint from the $T_{\text{eff}} - \log g$ diagram fit (2.25 to 2.7 Gyr, illustrated by the black error bar on the right side of Figure 19), then this restricts distance and extinction to $m - M = 7.25 - 7.4$ and $A_V = 0.2 - 0.3$. At 2.5 Gyr, $A_V = 0.25$ and $m - M = 7.35$, the τ^2 maximum-likelihood method derives values equal to those we determined with our 2D cross-correlation method.

4.6. Comparison between Padova, PARSEC and Dartmouth isochrone models

Many groups are developing stellar evolution models. While there is remarkable agreement between these models, there are noticeable departures especially around the turnoff and red giant branch due to choice of input physics and Solar composition (Dotter et al. 2008). In fact, the model choice is the greatest source of uncertainty when determining the fundamental properties of star clusters via isochrone fitting.

When we began our analysis, the Padova group provided the only models with synthetic MegaCam photometry. Since then, Dartmouth models have become available. Most recently, Padova has issued updated isochrones, which are now referred to as PARSEC models (Bressan et al. 2012): they have revised the major input physics, lowered the Solar metallicity from $Z = 0.019$ to $Z \approx 0.015$, and now include the pre-main sequence (irrelevant for this work).

The Padova (now PARSEC) webtool parameterizes composition with Z , where $[M/H] = \log(Z/Z_\odot)$. We used $Z = 0.022$ and 0.017 to query Padova and PARSEC models at $[M/H] \approx +0.065$. The Dartmouth webtool³⁴ uses $[Fe/H]$ instead of Z , and we set $[Fe/H] = +0.1$, according to the SME result for CWW 91. The left panel of Figure 20 shows that isochrones from Padova at 2.51 Gyr, PARSEC at 3.25 Gyr and Dartmouth at 3 Gyr map out the same sequence on the $T_{\text{eff}} - \log g$ diagram, except for the low mass departure at $\sim 0.8 M_\odot$ already noted. The middle and right panels plot the optical and NIR isochrones, with $A_V = 0.25$ and $m - M = 7.35$. The differences between models introduces an additional age uncertainty of at least 750 Myr. Assuming PARSEC more accurately models stellar evolution than their Padova predecessor, the difference between PARSEC and Dartmouth reduces the age uncertainty to only ~ 250 Myr. Figure 17 displays the results from fitting the 2MASS ($J - K_S$) CMD with Dartmouth $[Fe/H] = +0.1$ models, illustrated with the square symbols, and offset vertically from the Padova results by +0.06 for clarity. The peak is shifted to older ages relative to Padova, while the distance and extinction remain basically consistent – a consequence of the similarity between the 2.5 Gyr Padova model and 3 Gyr Dartmouth model in $T_{\text{eff}} - \log g$ space, and each group’s color – temperature transformations.

We will explore additional models (starting with BaSTI: Bag of Stellar Tracks and Isochrones, available at <http://albione.oa-teramo.inaf.it/>) in a more detailed analysis in a future work, where we intend to perform a simultaneous 7-band isochrone fit using our optical $g'r'i'z'$ 2MASS JHK_S , and our UKIRT JK photometry.

4.7. Distance: photometric versus astrometric

Dias et al. (2001) identified HIP 94635 (CWW 1) and HIP 94803 (CWW 2) as kinematic members of Ruprecht 147, and used their HIP1 parallaxes to derive a distance of 270 pc to the cluster. HIP1 lists $\pi = 3.57 \pm 1.01$ and 3.75 ± 1.04 mas for these stars respectively, while HIP2 provides larger values of 5.48 ± 0.65 and 4.92 ± 0.79 . Disregarding the advice of van Leeuwen (2007b) against deriving distances and distance moduli from parallaxes when the relative error is greater than 10%, one would

³³ code available at <http://www.astro.ex.ac.uk/people/timm/tau-squared>³⁴ <http://stellar.dartmouth.edu/models/>

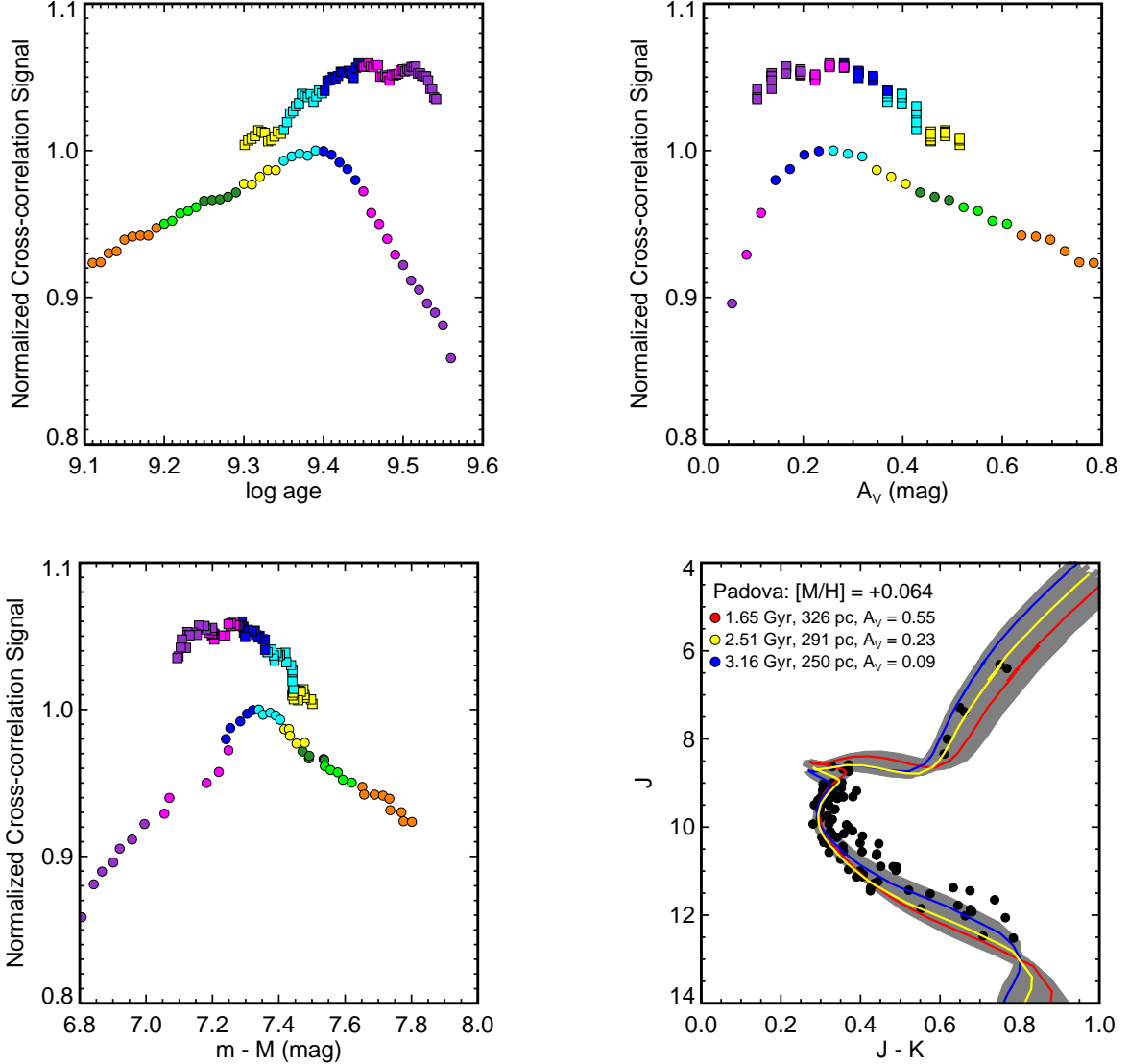


Figure 17. Isochrone fitting to NIR CMD with our 2D cross-correlation method: We tested Padova models (circles) with $\log t = 9.1$ to 9.6 (0.01 step size, ≈ 1.25 to 4 Gyr) and $[M/H] = +0.064$, and Dartmouth models (squares) with $[Fe/H] = +0.1$ with ages running from 2 to 3.5 Gyr. Our technique simulates stars clusters with 10^4 stars, including binaries, and computes the $m - M$ and A_V that best matches the R147 photometry. The model with maximum signal in each age / visual extinction / distance modulus bin (0.01, 0.05 mag., 0.025 mag.) is plotted in each panel, color coded according to age. We find that the model with the maximum cross-correlation signal has an age of 2.45 Gyr, $m - M = 7.34$ and $A_V = 0.26$. **Bottom - Right:** All solutions are plotted in gray along with R147 photometry as black points. Three models are highlighted: the best fit model (yellow), along with an older and younger model for reference. See §4.4 for more discussion.

determine a distance from HIP1 of 270 pc, and 193 pc from HIP2.

We also identify HIP 94435 (CWW 13) as a member of R147. Although HIP1 lists a discrepant parallax $\pi = 2.42 \pm 1.25$ (413 pc), HIP2 gives 4.64 ± 1.19 (216 pc) consistent with the other 2 HIP stars. While the HIP2 results are self-consistent, Figure 21 demonstrates there is simply no way an isochrone can be drawn through either the optical ($g' - i'$) or NIR ($J - K_S$) CMDs at the HIP2 distance moduli. The HIP2 parallax distances are all too close by ≈ 100 pc, compared to the photometric distances. This is reminiscent of the Pleiades problem, where the HIP1 parallax placed the cluster 0.23 mag. closer than distances inferred from main sequence fitting

and other methods. Soderblom et al. (2005) utilized the HST Fine Guidance Sensor to measure a new parallax distance consistent with the other non-HIP results.

5. FINAL SYNTHESIS AND SOURCES OF UNCERTAINTY

We have fit Padova isochrone models to three separate datasets: a $T_{\text{eff}} - \log g$ diagram consisting of 5 stars with values derived from SME, and both NIR ($J - K_S$) and optical ($g' - i'$) CMDs. We have chosen to use the Padova isochrones for our preliminary investigation into the properties of R147 because they provide colors in the MegaCam filter set. Other models (e.g. Dartmouth and Yonsei-Yale) show differences in the main sequence turnoff region, which provides the

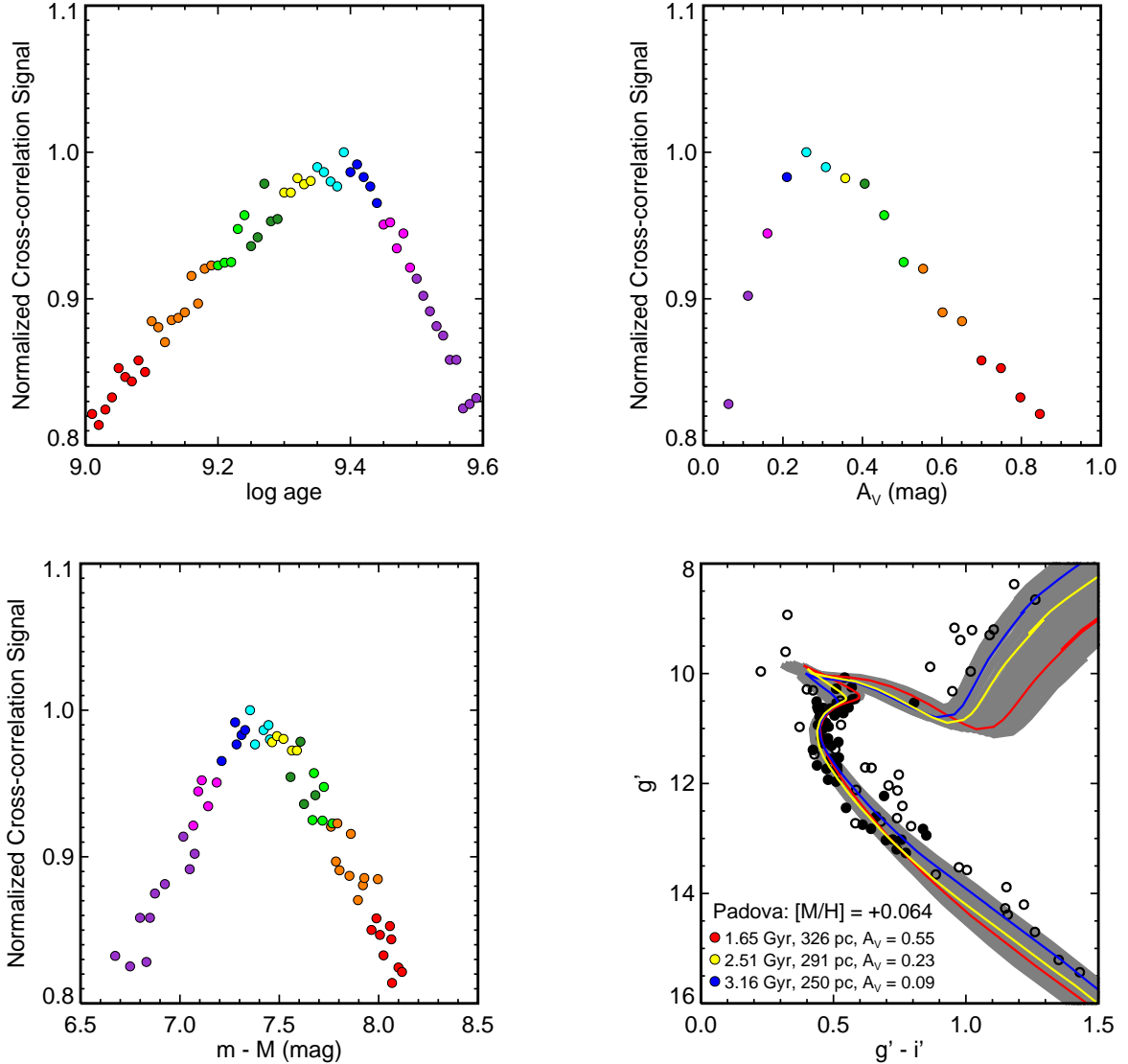


Figure 18. Similar to Figure 17, except we fit the optical CFHT/MegaCam ($g' - i'$) color – magnitude diagram, with the saturated red giants discarded (open circles). The lower K dwarfs were also removed (also open circles), because the Padova models are known to run hotter than the main sequence at $\sim 0.8 M_{\odot}$, as illustrated in Figure 20. We find that the model with the maximum cross-correlation signal has an age of 2.45 Gyr, $m - M = 7.35$ and $A_V = 0.26$. The isochrones plotted in the bottom – right panel have the following properties: Red – $\log t = 9.4$, $[M/H] = +0.08$, $m - M = 7.35$ and $A_V = 0.25$. Blue – $\log t = 9.53$, $[M/H] = +0.08$, $m - M = 6.92$ and $A_V = 0.11$. See §4.4 for more discussion. The fact that we derive essentially identical properties from our spectroscopic $T_{\text{eff}} - \log g$ diagram, and our NIR and optical CMDs validates the accuracy of the CFHT Elixir and TERAPIX photometric reduction (§2.5).

primary age constraint; and in the lower main sequence, where Padova runs bluer than Dartmouth and Yonsei-Yale. Our results, especially for age, therefore depend heavily on our chosen model.

Our solution is subject to additional sources of uncertainty, including photometric error, unresolved multiple star systems, and the possibility of differential extinction. Main sequence fitting, both to the single star and equal mass binary sequences, provides the primary constraint on the sum of distance and extinction. Ideally, these sequences would be vertically offset by 0.75 magnitudes (i.e. double the brightness), but for R147, there are separations of 1 magnitude or more. This unexpected offset could be explained by differential extinction, which would widen the sequence in both directions, by a pop-

ulation of triple systems, or if the stars are not actually cluster members. In this preliminary investigation, we have not yet untangled this δA_V – multiplicity – membership degeneracy on a star by star basis, but such an analysis would improve the precision of the cluster parameters.

At ~ 300 pc and $1^{\circ}.25$ in angular radius, we expect a physical radius of ~ 5 pc, which introduces a differential distance modulus of $\delta(m - M) = 0.02$ across the cluster. This is comparable to photometric error, and should be part of a more comprehensive error analysis.

While fitting the $T_{\text{eff}} - \log g$ diagram, assuming $[M/H] = +0.064$, we find $\log t = 9.4 \pm 0.03$, or $t = 2.5 \pm 0.02$ Gyr. If we increase or decrease the metallicity by ± 0.02 dex, the age error bars remain sim-

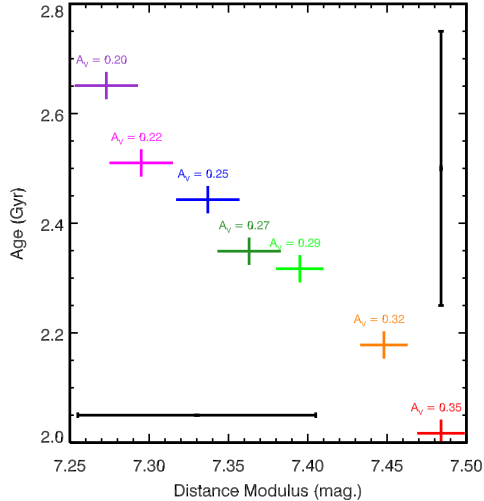


Figure 19. This plot illustrates the degeneracy between extinction, age and distance in isochrone fits to broadband photometry. Results are plotted from fitting 7 different A_V values with τ^2 , with $[M/H]$ fixed at +0.064 according to our SME analysis. All fits returned high τ^2 probabilities, and so model selection is only possible when we place additional constraints from our spectroscopic analysis. In Figure 15, we showed that a 5 star $T_{\text{eff}} - \log g$ diagram was best fit by a Padova isochrone with age = 2.5 ± 0.25 Gyr, illustrated by the error bar on the right side of this figure. This corresponds to a distance modulus of $m - M = 7.35 + 0.05 - 0.1$, shown by the error bar at the bottom of the figure, and $A_V = 0.25 + 0.08 - 0.05$. These properties are identical to the values we derived when fitting both the optical and NIR CMDs with our 2D cross-correlation technique, validating both our fitting method and the optical photometric reduction. See §4.5 for more discussion.

ilar and the best value for $\log t$ shifts by 0.02. When we performed the brute force SED fit to the early G dwarf for distance and extinction, we perturbed $[M/H]$ by ± 0.02 dex, $\log t$ by ± 0.5 , and T_{eff} by ± 50 K, and found $m - M = 7.44 \pm 0.06$ and $A_V = 0.25 \pm 0.04$.

For a given metallicity and extinction, τ^2 returns typical uncertainties of 40 – 100 Myr in age and 0.03 – 0.05 in distance modulus. Although the τ^2 code does calculate two diagnostics useful for model selection, the reduced τ^2 and a probability value, for the range of parameters we searched, the high degree of degeneracy between the four cluster parameters enabled τ^2 to find solutions which delivered high probabilities ($>60\%$) and reduced τ^2 values all ≈ 1 . Instead, we will select our preferred parameter set by fixing the metallicity according to our spectroscopic SME results: $[M/H] = +0.065$, and the age according to the $T_{\text{eff}} - \log g$ result at 2.5 Gyr. This breaks the degeneracy and we can then accept the corresponding distance and and visual extinction from τ^2 as best values: $m - M = 7.35$ ($d = 295$ pc) and $A_V = 0.25$.

This is essentially identical to our 2D cross-correlation results, where we found peak values at an age of 2.45 Gyr, $m - M = 7.34$ and $A_V = 0.26$, for the $[M/H] = +0.065$ case.

We set our preferred values with generous error bars at age = 2.5 ± 0.25 Gyr ($\log t = 9.4 \pm 0.03$), $[M/H] = 0.07 \pm 0.03$, $m - M = 7.25$ to 7.45 ($d = 280$ to 310 pc), and $A_V = 0.20$ to 0.30 . We set the metallicity error bars according to our SME analysis, ignoring the one anomalously low

metallicity result, and the hottest star with a poor χ^2_{ν} fit. We set the age and error bars according to our fit to the $T_{\text{eff}} - \log g$ diagram (Figure 15), which is corroborated by the 2D cross-correlation fit (Figure 18). We set the A_V range and lower bound $m - M$ value by placing these metallicity and age constraints on our τ^2 results (Figure 19). We extend the upper bound on $m - M$ past 7.4 to 7.45 mag. to encompass the result of our SED fit to the G0/2 dwarf. These results are summarized in Table 4, with the values of Kharchenko et al. (2005) and Pakhomov et al. (2009) provided for comparison.

6. SUMMARY, DISCUSSION AND UPCOMING WORK

Over 170 years passed since Herschel first cataloged Ruprecht 147 before astronomers finally investigated its properties and membership. Dias et al. and Kharchenko et al. demonstrated that a group of 20 – 40 stars at the location of R147 were in fact moving together in the plane of the sky, and estimated this group’s properties, although their analysis was hindered by $(B - V)$ photometry with a limiting magnitude near the main sequence turnoff. While Kharchenko et al. (2005) was able to determine an age (2.45 Gyr) from the MSTO consistent with the results of our analysis, the $(B - V)$ main sequence is dominated by photometric error and therefore provides a weak constraint on the distance, which their isochrone fitting has apparently placed 125 pc too close, at 175 pc compared to the 300 pc distance we find here. Nevertheless, these works by Dias et al. and Kharchenko et al. are significant because they essentially re-discovered R147. Pakhomov et al. (2009) first spectroscopically determined the composition for 3 red giant members, showing the cluster to be super-Solar (§1.2).

We queried the NOMAD catalog for stars within $1^\circ.5$ of the cluster center, and out of the 750,000 stars, we find 1348 with proper motion within 5 mas/yr of the R147 value (astrometric values from Kharchenko et al. 2005). We conducted an initial radial velocity survey at Lick and Palomar Observatories and for the first time confirm that over 100 stars are likely members of Ruprecht 147 and they are indeed moving together in three dimensions through the Galaxy (§2.2.3, 3.2). We followed up this initial survey with high resolution and signal-to-noise Ca II H & K spectra with MMT/Hectochelle, and used these second epoch RVs, at higher precision, to investigate binarity (§2.4, 3.4.3, 3.4.4). We have imaged the cluster in four optical bands (§2.5), and combined with 2MASS NIR photometry (§3.4.2), used the resulting CMDs to establish a membership list with 81 high-confidence members, 21 possible members, and 6 unlikely members (§3).

We have obtained high-resolution, high-SNR spectra of five members (§2.3), and determine the metallicity to be super-Solar using the SME spectral synthesis code, and find $[M/H] = +0.07 \pm 0.03$ and zero α -enhancement (§4.2).

We have fit Padova isochrones to the $T_{\text{eff}} - \log g$ diagram resulting from our spectroscopic analysis, and find that the age of R147 is best fit by a Padova isochrone with age of 2.5 Gyr (§4.3). $T_{\text{eff}} - \log g$ diagram isochrone fitting is independent of distance and visual extinction, which makes it a powerful tool, but this also means it does not directly provide any information on these pa-

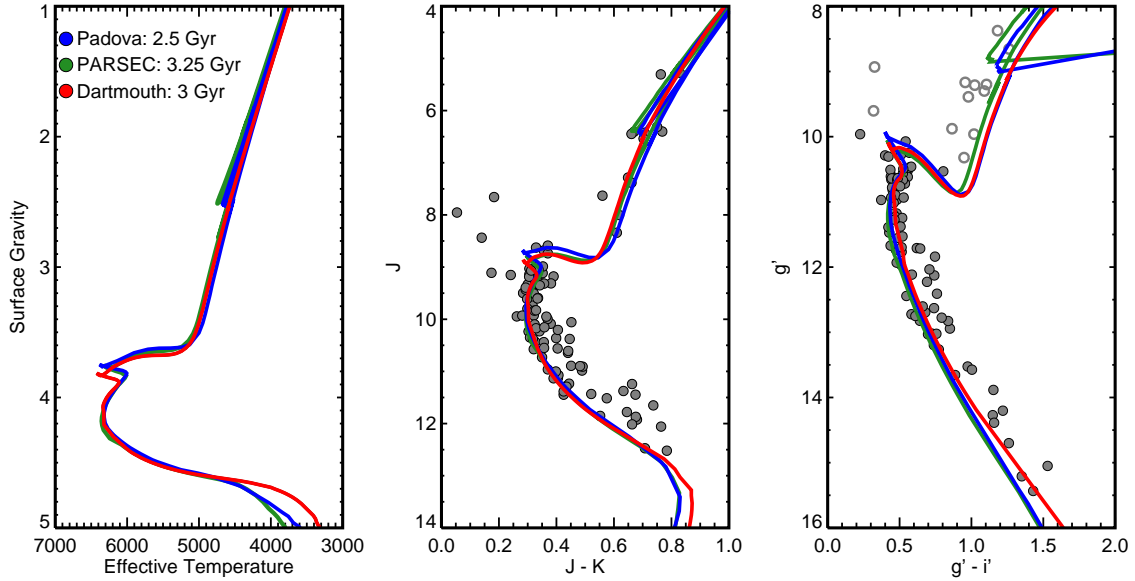


Figure 20. A Padova isochrone (blue, 2.5 Gyr, $[M/H] = +0.064$) is compared to the newly released PARSEC model (green, 3.25 Gyr) and a Dartmouth model (red, 3 Gyr), with metallicity set at $[M/H] \approx +0.06$. The Dartmouth age parameter must be increased by 500 Myr to match the Padova main sequence turnoff. The Padova lower main sequences are known to run hotter than many other stellar evolution models, diverging at approximately $0.8 M_{\odot}$. While this causes the Padova optical main sequence to undershoot the K dwarfs, the NIR sequence well matches the Dartmouth model until $0.7 M_{\odot}$. No stars below this mass were surveyed in this initial study, so the Padova models can be used to fit the entire NIR main sequence.

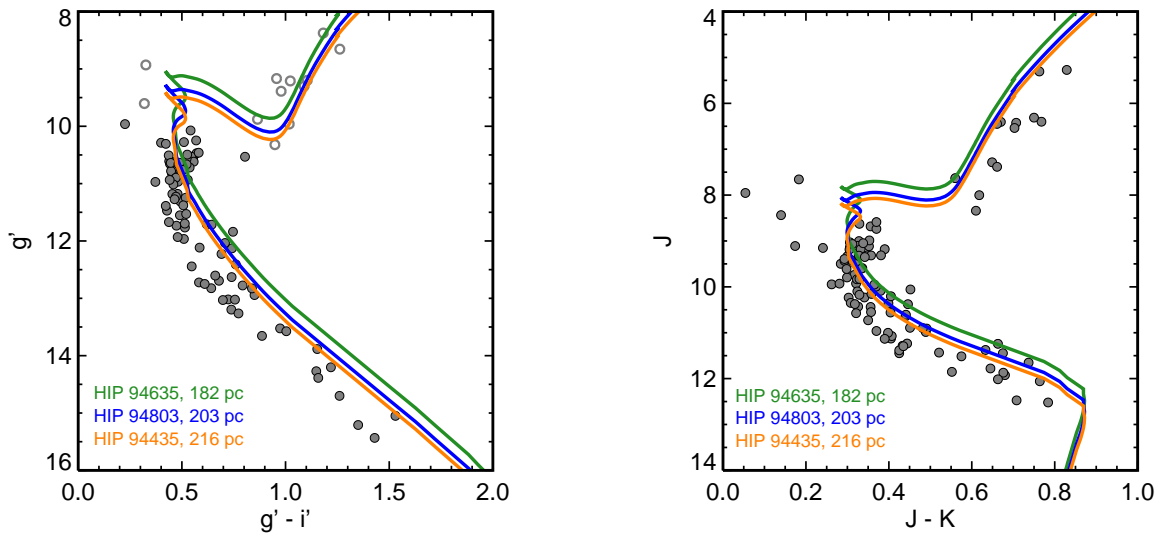


Figure 21. The R147 optical and NIR CMDs are plotted, along with Padova isochrones: 2.5 Gyr, $[M/H] = +0.064$, $A_V = 0.25$, and distance moduli corresponding to the HIP2 parallaxes for the 3 Hipparcos members: HIP 94635, 94803, and 94435 (CWW 1, 2, and 13). While the HIP2 parallaxes are all approximately in agreement, there is simply no way to place an isochrone at the distances implied by these parallaxes. We determine a photometric distance from optical and NIR isochrone fitting that is about 100 pc further than the HIP2 parallax distances, reminiscent of the Pleiades distance problem (Soderblom et al. 2005, see §4.7).

Table 4
Table of R147 cluster properties.

μ_α mas/yr	μ_δ mas/yr	RV ^a km s ⁻¹	Age ^b Gyr	Distance pc	A_V ^c mag.	Metallicity	Reference
-1.1	-27.3	41.1	2.51 ± 0.25	295 ± 15	0.25 ± 0.05	[M/H] = +0.07 ± 0.03	This work
-0.6	-27.7	41	2.45	175	0.47	...	Kharchenko et al. (2005)
...	...	40.5	1.26 ± 1.16	280 ± 100	0.34	FeI = 0.16, FeII = 0.08	Pakhomov et al. (2009)

Note. — Our proper motions are median values for ‘Y’ and ‘P’ members.

^a Our RV is the average of our 4 Keck velocities. Kharchenko et al.’s velocity is from Wilson (1953). Pakhomov et al.’s velocity is the average of the two apparent single stars. See Section 3.2.

^b All three groups determined ages from Padova isochrones. Our age is the best fit parameter from a fit to a $T_{\text{eff}} - \log g$ diagram (§4.3) and the NIR and optical CMDs and (§4.4). This parameter is heavily model-dependent: using PARSEC and Dartmouth models, we instead find 3.2 and 3 Gyr respectively (§4.6). Kharchenko et al. fit an optical ($B - V$) CMD with a Solar composition Padova model (Figure 4, §1.2). Pakhomov et al. determined composition, T_{eff} , and $\log g$ for 3 red giants from their high resolution spectroscopy, interpolated Padova models to the metallicities for each star, and fit for mass and age using their derived T_{eff} and $\log g$ values.

^c A_V assumes a $R_V = 3.1$ reddening law.

rameters. We queried the best fit Padova isochrone for a star with T_{eff} and $\log g$ closest to the values for the early G dwarf (CWW 91) we derived with SME, then performed a brute force SED fit to the resulting synthetic $g'r'i'JHK_S$ photometry, and find a minimum χ^2 at $m - M = 7.44$ (308 pc) and $A_V = 0.25$.

We consulted the dust map of Schlegel et al. (1998) to set an upper limit on the amount of visual extinction toward R147, $A_V < 0.5$ (§4.1), then fit Padova isochrones to the $(g' - i')$ and $(J - K_S)$ CMDs using a 2D cross-correlation technique developed here, which was inspired by and validated with the Naylor (2009) τ^2 maximum-likelihood method (§4.4). We find that without additional constraints from spectroscopy or additional photometric bands, just fitting a single CMD with isochrone models yields a suite of solutions all with high τ^2 probabilities, due to the high degree of degeneracy between age, composition, distance and visual extinction. If we break this degeneracy with the spectroscopic metallicity and age, we find $m - M = 7.33$ and $A_V = 0.23$ from τ^2 .

We found that the best models derived from fitting both $(J - K_S)$ and $(g' - i')$ CMDs with this technique corroborates the age we determined from the $T_{\text{eff}} - \log g$ fit, as well as the distance and extinction corresponding to this age in our τ^2 fits.

We recognize significant uncertainty in our solution from the unresolved binary population and possibility of differential extinction across this large cluster. These results are also heavily model-dependent (§4.6).

6.1. Discussion and Future Work

The R147 single star main sequence is not well defined, but blends smoothly into what is apparently the binary population. Evidently, R147 has a large binary fraction. The stellar population has encountered approximately 3 Gyr of Galactic gravitational tidal forces. Evaporation of the lightest-mass members should proceed first, both because low mass stars are preferentially ejected in 3-body encounters, and mass segregation gives them a larger effective radius and more susceptibility to Galactic tides. This process also preferentially ejects single stars from the cluster, as multiple star systems of similar spectral type have a greater bound mass. The ongoing dynamical evolution of an open cluster thus tends to increase the binary fraction, and we may be seeing this effect in the R147 main sequence.

Our membership list is top heavy, dominated by F stars (dwarfs, MSTO and subgiants) and red giants, with fewer numbers of G dwarfs, and only a handful of early K dwarfs. This dynamical evolution and evaporation could also explain the paucity of low mass members, and perhaps if any are left, they exist predominantly in multiples. But this can also be explained by observational bias: the NOMAD and UCAC-3 proper motion errors increase for the fainter members. These stars also begin to blend into the Galactic background in the color - magnitude diagrams, further complicating candidate identification. We are currently conducting a radial velocity survey for lower mass members, but this question will only finally be settled by deriving precise proper motions for the faint stars in the R147 field, which we intend to do by re-imaging the cluster with MegaCam in the near future.

If we are able to identify single M dwarfs, these will be

the only old (>1 Gyr), single cool dwarfs with known ages and compositions bright enough to admit close spectroscopic study. Once the white dwarf population is identified, it will provide an independent age estimate for the cluster and inform studies of white dwarf cooling curves. At 300 pc, chromospheric activity diagnostics are measurable, as is L_X , and R147 should prove useful for studying the evolution of angular momentum and magnetic activity at intermediate ages.

For these reasons and more, we will continue our efforts to characterize Ruprecht 147 and establish it as a new and important benchmark for stellar astrophysics.

J.L.C. acknowledges support from the National Science Foundation Graduate Research Fellowship Program supported by NSF grant No. DGE1255832, the Stephen B. Brumbach graduate fellowship, and the Zaccheus Daniel travel grant program. A.W. acknowledges a Hunter R. Rawlings III Cornell Presidential Research Scholarship.

J.T.W. conceived of and oversaw the project, and collected all of the candidate stellar spectra. A.W. and J.T.W. conducted the radial velocity survey at Palomar and Lick and produced the preliminary R147 membership list. J.M.B. conducted the SME analysis. J.A.J. was PI on the program that obtained the optical photometry from CFHT/MegaCam, and also conducted preliminary SME analysis of Lick and Keck spectra to determine the composition of R147 (results are not reported in this work, though they informed this study). J.L.C. and J.T.W. performed the Hectochelle RV survey. J.L.C. was primarily responsible for the writing of the manuscript and the final analysis and synthesis of all data.

We would like to thank Gabor Fűrész and Andrew Szentgyorgyi for assisting the Hectochelle data reduction; Tim Naylor for assisting us with his τ^2 code; Aaron Dotter for providing access to the Dartmouth isochrones with the CFHT/MegaCam filters; David Monet and Stephen Levine for providing the NOMAD catalog on HDD; James Graham and James Lloyd for supporting this research; Matthew Muterspaugh for sharing and swapping Lick 3-m time; and Kevin Covey for providing extensive comments on an early draft of this paper. We would also like to thank all observing staff and telescope operators at MMT/FLWO, CFHT, Lick, Palomar, and Keck; and Geoff Marcy, Andrew Howard and the California Planet Survey observing team for their assistance in acquiring the Keck spectra. We also appreciate our anonymous referee for offering thorough and constructive suggestions that improved this paper. Finally, we thank Debra Fischer, Jeff Valenti, Adam Kraus, Steve Saar, Søren Meibom, Andrew West, Kevin Covey, Marcel Agüeros, Suzanne Hawley, Ivan King, Jay Anderson, Bob Mathieu, Ken Janes, and Eric Mamajek for helpful conversations, suggestions, and support.

This work is based on observations obtained with MegaCam, a joint project of CFHT and CEA/DAPNIA, at the Canada-France-Hawaii Telescope (CFHT) which is operated by the National Research Council (NRC) of Canada, the Institut National des Sciences de l'Univers of the Centre National de la Recherche Scientifique of France, and the University of Hawaii. Observing time was granted by the University of Hawaii Institute for Astronomy TAC. These data were reduced at the TER-

APIX data center located at the Institut d’Astrophysique de Paris.

Observations reported here were obtained at the MMT Observatory, a joint facility of the Smithsonian Institution and the University of Arizona. MMT telescope time was granted by NOAO (Project PA-10A-0378, PI J. Wright), through the Telescope System Instrumentation Program (TSIP). TSIP is funded by NSF.

This publication makes use of data products from the Two Micron All Sky Survey, which is a joint project of the University of Massachusetts and the Infrared Processing and Analysis Center/California Institute of Technology, funded by NASA and the NSF.

Some of the data presented herein were obtained at the W.M. Keck Observatory, which is operated as a scientific partnership among the California Institute of Technology, the University of California and the National Aeronautics and Space Administration. The Observatory was made possible by the generous financial support of the W.M. Keck Foundation. The authors wish to recognize and acknowledge the very significant cultural role and reverence that the summit of Mauna Kea has always had within the indigenous Hawaiian community. We are most fortunate to have the opportunity to conduct observations from this mountain.

This research made use of Montage, funded by NASA’s Earth Science Technology Office, Computation Technologies Project, under Cooperative Agreement Number NCC5-626 between NASA and the California Institute of Technology. Montage is maintained by the NASA/IPAC Infrared Science Archive.

This research made use of the WEBDA database operated at the Institute for Astronomy of the University of Vienna, NASAs Astrophysics Data System Bibliographic Services, and the SIMBAD database and the Vizier catalogue access tool operated at CDS, Strasbourg, France.

Any opinions, findings, and conclusions or recommendations expressed in this material are those of the authors and do not necessarily reflect the views of the National Science Foundation or any other institute cited above.

Facilities: Shane, Hale, MMT, CFHT, Keck:I

REFERENCES

- Agüeros, M. A. et al. 2011, *ApJ*, 740, 110
- Alter, G., Ruprecht, J., & Vanysek, J. 1958, *Catalogue of star clusters and associations*, ed. G. Alter, J. Ruprecht, & J. Vanysek
- Archinal, B. A., & Hynes, S. J. 2003, *Star clusters*
- Bertin, E. 2006, in *Astronomical Society of the Pacific Conference Series*, Vol. 351, *Astronomical Data Analysis Software and Systems XV*, ed. C. Gabriel, C. Arviset, D. Ponz, & S. Enrique, 112
- Bertin, E., Mellier, Y., Radovich, M., Missonnier, G., Didelon, P., & Morin, B. 2002, in *Astronomical Society of the Pacific Conference Series*, Vol. 281, *Astronomical Data Analysis Software and Systems XI*, ed. D. A. Bohlender, D. Durand, & T. H. Handley, 228
- Bressan, A., Marigo, P., Girardi, L., Salasnich, B., Dal Cero, C., Rubele, S., & Nanni, A. 2012, *ArXiv e-prints*
- Burnham, R. 1966, *Burnham’s celestial handbook; an observer’s guide to the universe beyond the solar system. A descriptive catalog and reference handbook of deep-sky wonders for the observer, student, research worker, amateur or professional astronomer.*, ed. Burnham, R.
- Cardelli, J. A., Clayton, G. C., & Mathis, J. S. 1989, *ApJ*, 345, 245
- Chubak, C., Marcy, G., Fischer, D. A., Howard, A. W., Isaacson, H., Johnson, J. A., & Wright, J. T. 2012, *ArXiv e-prints*
- Dias, W. S., Alessi, B. S., Moitinho, A., & Lépine, J. R. D. 2002, *A&A*, 389, 871
- Dias, W. S., Assafin, M., Flório, V., Alessi, B. S., & LÍbero, V. 2006, *A&A*, 446, 949
- Dias, W. S., Lépine, J. R. D., & Alessi, B. S. 2001, *A&A*, 376, 441
- Dotter, A., Chaboyer, B., Jevremović, D., Kostov, V., Baron, E., & Ferguson, J. W. 2008, *ApJS*, 178, 89
- Dreyer, J. L. E. 1888, *MmRAS*, 49, 1
- Drimmel, R., & Spergel, D. N. 2001, *ApJ*, 556, 181
- Elsanhoury, W. H., Hamdy, M. A., Nough, M. I., Saad, A. S., & Saad, S. M. 2011, *ISRN Astronomy and Astrophysics*, vol. 2011, id.#127030, 2011
- Fabricant, D. et al. 2004, in *Presented at the Society of Photo-Optical Instrumentation Engineers (SPIE) Conference*, Vol. 5492, *Society of Photo-Optical Instrumentation Engineers (SPIE) Conference Series*, ed. A. F. M. Moorwood & M. Iye, 767–778
- Fuhrmann, K., Pfeiffer, M., Frank, C., Reetz, J., & Gehren, T. 1997, *A&A*, 323, 909
- Fűrész, G., Szentgyorgyi, A. H., & Meibom, S. 2008, in *Precision Spectroscopy in Astrophysics*, ed. N. C. Santos, L. Pasquini, A. C. M. Correia, & M. Romaniello, 287–290
- Girardi, L., Bressan, A., Bertelli, G., & Chiosi, C. 2000, *A&AS*, 141, 371
- Herschel, J. F. W. 1833, *Philosophical Transactions of the Royal Society of London*, 123, 359
- . 1863, *Royal Society of London Proceedings Series I*, 13, 1
- Høg, E. et al. 2000, *A&A*, 355, L27
- Hora, J. L., Luppino, G. A., & Hodapp, K.-W. 1994, in *Society of Photo-Optical Instrumentation Engineers (SPIE) Conference Series*, Vol. 2198, *Society of Photo-Optical Instrumentation Engineers (SPIE) Conference Series*, ed. D. L. Crawford & E. R. Craine, 498–503
- Jones, D. O., West, A. A., & Foster, J. B. 2011, *AJ*, 142, 44
- Kharchenko, N. V. 2001, *Kinematika i Fizika Nebesnykh Tel*, 17, 409
- Kharchenko, N. V., Piskunov, A. E., Röser, S., Schilbach, E., & Scholz, R. 2005, *A&A*, 438, 1163
- Lallement, R., Welsh, B. Y., Vergely, J. L., Crifo, F., & Sfeir, D. 2003, *A&A*, 411, 447
- Landsman, W., Aparicio, J., Bergeron, P., Di Stefano, R., & Stecher, T. P. 1997, *ApJ*, 481, L93
- Lynge, G., & Palous, J. 1987, *A&A*, 188, 35
- Magnier, E. A., & Cuillandre, J.-C. 2002, in *Society of Photo-Optical Instrumentation Engineers (SPIE) Conference Series*, Vol. 4844, *Society of Photo-Optical Instrumentation Engineers (SPIE) Conference Series*, ed. P. J. Quinn, 343–350
- Marigo, P., Girardi, L., Bressan, A., Groenewegen, M. A. T., Silva, L., & Granato, G. L. 2008, *A&A*, 482, 883
- Mathieu, R. D. 1983, *PhD thesis, California Univ., Berkeley.*
- Mathieu, R. D., Latham, D. W., & Griffin, R. F. 1990, *AJ*, 100, 1859
- Meibom, S. et al. 2011, *ApJ*, 733, L9
- Mermilliod, J. 1995, in *Astrophysics and Space Science Library*, Vol. 203, *Information & On-Line Data in Astronomy*, ed. D. Egret & M. A. Albrecht, 127–138
- Mermilliod, J., & Paunzen, E. 2003, *A&A*, 410, 511
- Mink, D. J., Wyatt, W. F., Caldwell, N., Conroy, M. A., Furesz, G., & Tokarz, S. P. 2007, in *Astronomical Society of the Pacific Conference Series*, Vol. 376, *Astronomical Data Analysis Software and Systems XVI*, ed. R. A. Shaw, F. Hill, & D. J. Bell, 249–+
- Monet, D. G. et al. 2003, *AJ*, 125, 984
- Naylor, T. 2009, *MNRAS*, 399, 432
- Naylor, T., & Jeffries, R. D. 2006, *MNRAS*, 373, 1251
- Nidever, D. L., Marcy, G. W., Butler, R. P., Fischer, D. A., & Vogt, S. S. 2002, *ApJS*, 141, 503
- Norris, J. M., Wright, J. T., Wade, R. A., Mahadevan, S., & Gettel, S. 2011, *ApJ*, 743, 88
- Pakhomov, Y. V., Antipova, L. I., Boyarchuk, A. A., Bizyaev, D. V., Zhao, G., & Liang, Y. 2009, *Astronomy Reports*, 53, 660
- Peri, M. L. 1995, *PhD thesis, AA(California Inst. of Tech.)*

- Perryman, M. A. C., & ESA. 1997, The HIPPARCOS and TYCHO catalogues. Astrometric and photometric star catalogues derived from the ESA HIPPARCOS Space Astrometry Mission (The Hipparcos and Tycho catalogues. Astrometric and photometric star catalogues derived from the ESA Hipparcos Space Astrometry Mission, Publisher: Noordwijk, Netherlands: ESA Publications Division, 1997, Series: ESA SP Series vol no: 1200, ISBN: 9290923997 (set))
- Pichardo, B., Moreno, E., Allen, C., Bedin, L. R., Bellini, A., & Pasquini, L. 2012, *AJ*, 143, 73
- Roeser, S., Demleitner, M., & Schilbach, E. 2010, *AJ*, 139, 2440
- Ruprecht, J. 1966, *Bulletin of the Astronomical Institutes of Czechoslovakia*, 17, 33
- Sanders, W. L. 1971, *A&A*, 14, 226
- Schilbach, E., Kharchenko, N. V., Piskunov, A. E., Röser, S., & Scholz, R.-D. 2006, *A&A*, 456, 523
- Schlegel, D. J., Finkbeiner, D. P., & Davis, M. 1998, *ApJ*, 500, 525
- Skrutskie, M. F. et al. 2006, *AJ*, 131, 1163
- Soderblom, D. R. 2010, *ARA&A*, 48, 581
- Soderblom, D. R., Nelan, E., Benedict, G. F., McArthur, B., Ramirez, I., Spiesman, W., & Jones, B. F. 2005, *AJ*, 129, 1616
- Szentgyorgyi, A. H., Cheimets, P., Eng, R., Fabricant, D. G., Geary, J. C., Hartmann, L., Pieri, M. R., & Roll, J. B. 1998, in *Society of Photo-Optical Instrumentation Engineers (SPIE) Conference Series*, Vol. 3355, *Society of Photo-Optical Instrumentation Engineers (SPIE) Conference Series*, ed. S. D'Odorico, 242–252
- Thackeray, A. D. 1939, *MNRAS*, 99, 492
- Trumpler, R. J. 1930, *Lick Observatory Bulletin*, 14, 154
- Valenti, J. A., & Fischer, D. A. 2005, *ApJS*, 159, 141
- Valenti, J. A., & Piskunov, N. 1996, *A&AS*, 118, 595
- van Leeuwen, F., ed. 2007a, *Astrophysics and Space Science Library*, Vol. 350, *Hipparcos, the New Reduction of the Raw Data*
- . 2007b, *Astrophysics and Space Science Library*, Vol. 350, *Hipparcos, the New Reduction of the Raw Data*
- Vogt, S. S. 1987, *PASP*, 99, 1214
- Vogt, S. S. et al. 1994, in *Proc. SPIE Instrumentation in Astronomy VIII*, David L. Crawford; Eric R. Craine; Eds., Volume 2198, p. 362, 362–+
- Wilson, O. C., & Vainu Bappu, M. K. 1957, *ApJ*, 125, 661
- Wilson, R. E. 1953, *Carnegie Institute Washington D.C. Publication*, 0
- Wright, J. T., Marcy, G. W., Butler, R. P., & Vogt, S. S. 2004, *ApJS*, 152, 261
- Zacharias, N. et al. 2009, *VizieR Online Data Catalog*, 1315, 0
- Zacharias, N., Monet, D. G., Levine, S. E., Urban, S. E., Gaume, R., & Wycoff, G. L. 2004a, in *Bulletin of the American Astronomical Society*, Vol. 36, *Bulletin of the American Astronomical Society*, 1418–+
- Zacharias, N., Urban, S. E., Zacharias, M. I., Wycoff, G. L., Hall, D. M., Monet, D. G., & Rafferty, T. J. 2004b, *AJ*, 127, 3043
- Zhu, Z. 2009, *Research in Astronomy and Astrophysics*, 9, 1285
- Zombeck, M. 2007, *Handbook of Space Astronomy and Astrophysics: Third Edition*, ed. Zombeck, M. (Cambridge University Press)

Table 5
Membership list

CWW ID	2MASS ID	$\mu_{RA}(\sigma_\mu)$	$\mu_{Dec}(\sigma_\mu)$	g'	$g' - i'$	J^a	$J - K_S^a$	RV_{LP}	RV_H	Mem. ^b	MemFlag ^c	Notes ^d
1	19152612-1605571	-1.0 (0.7)	-27.4 (0.6)	8.37	1.18	5.31	0.76	38.5	-	Y	YP-YY	RG
2	19172384-1604243	-2.2 (0.8)	-27.6 (0.6)	8.66	1.26	5.27	0.83	43.4	-	Y	YY-YY	RG
3	19161966-1634094	-1.5 (1.6)	-25.4 (1.5)	8.65	-0.10	8.05	-0.02	-	-	Y	Y- -BB	BS
4	19171130-1603082	-0.9 (1.5)	-29.1 (1.5)	9.20	1.10	6.40	0.77	42.7	41.1	Y	YYYYY	RG
5	19164073-1616411	-0.3 (1.6)	-25.4 (1.5)	8.81	-0.04	7.95	0.05	-	-	Y	Y- -BB	BS
6	19170343-1703138	-0.7 (1.9)	-30.1 (1.8)	9.21	1.02	6.42	0.71	46.2	-	Y	YY-YY	RG
7	19183747-1712575	-0.4 (1.9)	-26.7 (1.8)	-	-	6.41	0.67	42.4	-	Y	YY-Y-	
8	19181439-1641226	1.8 (1.5)	-25.3 (1.5)	8.93	0.33	7.66	0.18	-	-	Y	Y- -BB	BS
9	19140272-1554055	-0.4 (1.5)	-26.1 (1.4)	9.30	1.09	6.31	0.75	42.1	-	Y	YY-YY	RG/SB1?
10	19155129-1617591	-2.7 (1.6)	-26.8 (1.5)	9.17	0.96	6.45	0.66	41.4	40.6	Y	YYYYY	RG
11	19180978-1616222	-1.4 (1.5)	-27.3 (1.5)	9.39	0.98	6.54	0.70	44.2	-	Y	YY-YY	RG
12	19164388-1626239	-1.2 (1.6)	-24.6 (1.5)	9.60	0.32	8.44	0.14	-	-	Y	Y- -BB	BS
13	19131526-1706210	-0.1 (1.1)	-27.1 (0.8)	-	-	7.28	0.65	46.4	-	Y	YY-Y-	
14	19134817-1650059	-1.5 (1.4)	-26.2 (1.3)	9.88	0.87	7.63	0.56	43.6	-	Y	YY-YY	RG
15	19164574-1635226	-1.6 (1.6)	-27.1 (1.5)	9.96	1.02	7.38	0.66	46.1	41.4	Y	YYYYY	RG
16	19164823-1611522	1.9 (1.6)	-26.1 (1.7)	9.96	0.23	9.11	0.17	-	-	Y	Y- -BB	BS
17	19165670-1612265	-1.7 (1.7)	-26.8 (1.8)	10.07	0.54	8.59	0.37	44.2	40.6	Y	YYYYY	
18	19193373-1658514	0.3 (4.2)	-26.2 (4.7)	-	-	8.68	0.36	47.2	-	Y	YP-Y-	
19	19161456-1624071	-0.2 (2.0)	-28.6 (2.0)	10.32	0.95	8.00	0.62	43.8	43.9	P	YYPYY	RG
20	19160865-1611148	-3.4 (1.6)	-29.3 (1.8)	10.25	0.57	8.63	0.33	41.8	41.7	Y	YYYYY	
21	19132220-1645096	-5.4 (1.5)	-29.1 (1.6)	10.28	0.51	8.74	0.37	41.9	-	Y	YY-YY	
22	19172382-1612488	-1.7 (1.7)	-30.8 (1.8)	10.31	0.42	9.26	0.44	51.9	38.2	P	YNNYY	SB1
23	19154269-1633050	-1.8 (2.2)	-30.3 (2.3)	11.67	0.44	10.38	0.32	34.7	41.2	Y	YNNYY	SB1?
24	19172865-1633313	1.1 (1.7)	-27.6 (1.8)	10.29	0.40	9.11	0.21	41.8	-	Y	YY-YB	BS?
25	19133648-1548104	-1.4 (1.4)	-28.5 (1.5)	10.53	0.80	8.34	0.61	40.7	-	Y	YY-YY	RG
26	19153282-1620388	0.2 (1.8)	-27.1 (2.0)	10.51	0.44	9.03	0.31	46.1	42.0	Y	YYYYY	
27	19171984-1607383	-2.0 (1.9)	-30.8 (2.0)	10.46	0.58	8.96	0.29	48.3	48.4	P	YPNYY	
28	19152638-1700159	-2.1 (2.0)	-29.6 (2.3)	10.53	0.56	9.08	0.24	43.9	-	Y	YY-YY	
29	19173931-1636348	1.2 (1.6)	-25.4 (1.6)	10.47	0.57	9.00	0.33	41.6	-	Y	YY-YY	
30	19155841-1615258	-2.8 (1.9)	-28.9 (2.1)	10.57	0.52	9.20	0.39	41.4	40.7	Y	YYPYY	
31	19195154-1603583	-2.4 (2.0)	-27.3 (2.2)	-	-	9.05	0.34	41.7	-	Y	YY-Y-	
32	19151540-1619517	-1.8 (1.8)	-26.8 (2.1)	10.70	0.52	9.30	0.33	45.9	42.2	Y	YYYYY	
33	19181155-1629141	1.4 (1.9)	-27.0 (1.9)	10.66	0.44	9.39	0.29	41.2	-	Y	YY-YY	
34	19165477-1702129	3.2 (3.2)	-28.7 (3.5)	10.63	0.46	9.41	0.31	45.8	-	Y	YY-YY	
35	19163976-1626316	0.1 (1.9)	-24.8 (2.1)	10.53	0.55	9.10	0.32	45.1	41.1	Y	YYYYY	
36	19153626-1557460	-0.7 (1.9)	-27.2 (2.1)	10.49	0.53	9.07	0.31	46.4	41.8	Y	YYYYY	
37	19163344-1607515	-2.5 (2.1)	-27.6 (2.2)	10.64	0.49	9.32	0.36	34.6	41.0	Y	YNNYY	
38	19142651-1606340	-2.5 (2.0)	-27.2 (2.1)	10.66	0.48	9.33	0.41	45.1	41.2	Y	YYPYY	
39	19150275-1609405	-5.2 (1.9)	-28.3 (2.1)	10.66	0.52	9.19	0.31	42.7	41.7	Y	YYYYY	
40	19163339-1620215	-3.0 (1.9)	-24.9 (2.1)	10.62	0.56	9.18	0.33	42.1	41.5	Y	YYYYY	
41	19170481-1636526	4.3 (2.0)	-28.6 (2.2)	10.61	0.44	9.33	0.30	45.9	-	Y	YY-YY	
42	19183120-1614421	-1.8 (2.2)	-26.9 (2.2)	10.64	0.45	9.32	0.33	44.6	-	Y	YY-YY	
43	19180054-1636016	1.3 (1.9)	-26.3 (2.0)	10.70	0.46	9.44	0.27	44.9	-	Y	YY-YY	
44	19164495-1717074	2.7 (2.3)	-27.2 (2.5)	10.97	0.48	9.74	0.32	42.2	-	Y	YY-YY	
45	19150860-1657412	-2.0 (2.0)	-30.0 (2.3)	10.82	0.45	9.50	0.28	45.7	-	Y	YY-YY	
46	19163525-1705075	3.7 (2.3)	-28.0 (2.6)	10.80	0.46	9.52	0.30	45.5	-	Y	YY-YY	
47	19131541-1616123	-5.6 (1.7)	-30.0 (1.8)	10.78	0.45	9.51	0.32	44.5	-	Y	YY-YY	
48	19164662-1619208	0.0 (2.1)	-26.4 (2.2)	10.72	0.54	9.34	0.37	46.3	42.3	Y	YYYYY	
49	19142907-1549056	0.3 (1.9)	-25.3 (2.1)	10.76	0.50	9.36	0.36	46.2	-	Y	YY-YY	
50	19162934-1645544	-2.4 (2.0)	-27.4 (2.3)	10.97	0.37	9.80	0.30	47.6	-	P	YP-YP	
51	19163620-1607363	-3.0 (2.5)	-29.5 (2.6)	11.02	0.46	9.12 ^e	0.35	44.9	-	Y	YY-YY	
52	19162169-1609510	-0.9 (2.1)	-27.7 (2.3)	10.90	0.47	9.59	0.34	39.2	40.1	Y	YYYYY	
53	19163231-1611346	-2.8 (2.2)	-29.3 (2.3)	10.93	0.53	9.60	0.33	46.9	45.2	P	YNNYP	
54	19165573-1603220	-0.8 (2.2)	-30.2 (2.4)	11.39	0.42	10.10	0.32	48.9	42.8	Y	YPPYY	
55	19160452-1605313	-0.6 (2.1)	-32.1 (2.2)	10.94	0.44	9.61	0.30	45.4	41.8	Y	YYYYY	

Table 5 — *Continued*

CWW ID	2MASS ID	$\mu_{\text{RA}}(\sigma_{\mu})$	$\mu_{\text{Dec}}(\sigma_{\mu})$	g'	$g' - i'$	J ^a	$J - K_S$ ^a	RV_{LP}	RV_{H}	Mem. ^b	MemFlag ^c	Notes ^d
56	19200522-1535360	1.1 (1.9)	-25.8 (2.0)	-	-	9.83	0.33	40.7	-	Y	YY-Y-	
57	19170433-1623185	-0.2 (2.2)	-28.6 (2.3)	11.23	0.47	9.93	0.27	41.9	41.8	Y	YYYYY	
58	19172172-1535592	-0.4 (1.7)	-28.1 (1.7)	11.27	0.46	9.95	0.36	44.6	-	Y	YY-PY	
59	19151260-1705121	2.9 (2.5)	-30.6 (2.7)	11.18	0.48	9.92	0.24	50.1	-	P	YP-PY	
60	19114731-1632485	0.8 (2.2)	-27.1 (2.3)	11.31	0.49	10.09	0.38	43.5	-	Y	YY-PY	
61	19145840-1650089	-4.5 (2.2)	-29.1 (2.3)	11.18	0.45	9.93	0.32	42.2	-	Y	YY-YY	
62	19164922-1613222	-0.5 (2.2)	-24.9 (2.3)	11.25	0.52	9.84	0.32	45.0	42.5	Y	YYYYY	
63	19152981-1551047	-1.8 (1.7)	-26.5 (1.8)	11.53	0.52	10.17	0.33	39.7	41.4	Y	YYYYY	
64	19152465-1651222	-1.5 (2.4)	-26.1 (2.5)	11.72	0.64	10.20	0.40	-	-	P	Y-PP	SB2
65	19164440-1615338	-3.6 (3.7)	-23.7 (3.7)	13.88	1.15	11.45	0.68	-	-	Y	Y-PY	SB2
66	19150050-1614245	-1.5 (2.2)	-27.5 (2.3)	11.71	0.62	10.15	0.36	-	-	P	Y-YP	SB2
67	19151498-1720177	-0.1 (2.5)	-29.1 (2.8)	11.84	0.75	10.08	0.47	34.7	-	N	YN-NN	
68	19180536-1646438	3.4 (3.7)	-29.8 (3.7)	13.57	1.00	11.25	0.67	-	-	Y	Y-PY	SB2
69	19161864-1611305	-6.8 (2.2)	-30.6 (2.3)	11.38	0.51	9.99	0.37	42.4	37.2	P	PYNPY	
70	19163827-1625039	1.1 (2.2)	-29.6 (2.3)	11.47	0.43	10.23	0.30	37.9	38.9	P	YPPYY	
71	19154511-1623157	-0.1 (2.2)	-27.0 (2.4)	11.93	0.48	10.57	0.32	41.4	41.1	Y	YYYYY	
72	19165800-1614277	-2.6 (2.3)	-30.8 (2.4)	12.04	0.71	10.36	0.40	47.9	46.6	P	YPNYP	SB2
73	19160523-1652561	-3.5 (2.4)	-26.8 (2.4)	11.73	0.47	10.43	0.33	42.5	-	Y	YY-YY	
74	19150925-1552241	-0.1 (1.8)	-28.6 (1.8)	11.55	0.49	10.23	0.34	42.1	42.2	Y	YYYYY	
75	19161121-1621485	4.2 (3.6)	-25.5 (3.6)	13.20	0.74	11.43	0.52	39.5	42.2	Y	YYYYY	
76	19134334-1649109	6.6 (3.8)	-77.7 (3.8)	12.69	0.68	11.13	0.41	43.5	-	P	NY-YY	
77	19150012-1605517	-0.4 (3.2)	-25.0 (3.2)	12.12	0.59	10.56	0.40	50.5	52.6	N	YNNYY	
78	19160879-1524279	-3.8 (2.0)	-30.5 (2.1)	11.70	0.51	10.35	0.31	40.8	-	Y	YY-YY	
79	19142816-1620023	-2.6 (3.0)	-28.6 (3.1)	12.60	0.66	11.00	0.40	42.3	42.1	Y	YYYYY	
80	19162501-1632018	-2.0 (2.4)	-29.5 (2.5)	12.13	0.74	10.38	0.45	41.5	-	P	YY-PP	
81	19151897-1639244	-2.1 (2.2)	-25.5 (2.4)	11.77	0.51	10.44	0.36	41.2	-	Y	YY-YY	
82	19152406-1621519	-1.3 (2.4)	-29.6 (2.4)	11.97	0.51	10.55	0.36	47.9	42.5	Y	YPPYY	
83	19134126-1610201	-5.3 (3.2)	-29.5 (3.3)	12.23	0.69	10.64	0.44	42.0	-	Y	YY-YY	
84	19141294-1554291	-1.8 (3.1)	-26.6 (2.9)	12.41	0.76	10.61	0.44	46.7	-	Y	YY-YY	
85	19165940-1635271	-2.8 (3.1)	-27.7 (3.1)	12.82	0.64	11.23	0.44	42.6	42.9	Y	YYYYY	
86	19160589-1629481	-0.3 (2.9)	-28.7 (2.9)	12.94	0.85	10.98	0.49	44.7	41.6	Y	YYYYY	
87	19160785-1610360	-4.5 (2.9)	-26.8 (3.0)	12.83	0.84	10.91	0.49	45.0	42.4	Y	YYYYY	
88	19162477-1710375	-4.3 (3.7)	-42.8 (3.7)	13.02	0.72	11.28	0.43	47.0	-	P	PY-YY	
89	19173402-1652177	-1.6 (2.5)	-31.9 (2.5)	12.72	0.58	11.07	0.41	47.3	-	P	YP-YY	
90	19163672-1713101	-0.1 (2.9)	-31.8 (2.9)	12.44	0.55	10.95	0.32	42.0	-	Y	YY-YY	
91	19164725-1604093	-2.2 (3.1)	-29.5 (3.0)	12.75	0.61	11.13	0.36	42.8	42.2	Y	YYYYY	
92	19164417-1612222	-1.5 (3.6)	-29.0 (3.6)	12.63	0.74	10.89	0.45	45.1	25.2	P	YNNYY	SB1
93	19162203-1546159	1.5 (2.9)	-27.6 (2.9)	13.02	0.76	11.29	0.43	41.8	41.7	Y	YYYYY	
94	19152141-1600107	-2.6 (3.2)	-27.1 (3.2)	13.26	0.77	11.43	0.38	43.5	42.8	Y	YYYPY	
95	19170128-1609423	-1.5 (2.9)	-30.1 (2.9)	12.78	0.79	10.90	0.48	40.6	39.1	P	YPPYY	
96	19151156-1726308	-0.5 (2.1)	-27.0 (2.1)	-	-	10.73	0.35	40.8	-	Y	YY-Y-	
97	19170285-1605166	-1.7 (3.6)	-27.9 (3.6)	13.03	0.70	11.38	0.43	40.9	41.1	Y	YYYYY	
98	19162656-1614545	0.4 (2.9)	-29.5 (2.9)	13.52	0.97	11.38	0.63	43.2	40.7	Y	YYYPY	
99	19161757-1600177	-2.4 (3.0)	-29.4 (3.0)	13.66	0.89	11.52	0.58	44.8	44.6	P	YNNYY	
100	19145199-1541379	0.2 (3.7)	-3.7 (3.7)	14.20	1.22	11.67	0.79	42.2	-	N	NY-PY	
101	19153354-1625368	-9.0 (3.7)	-31.6 (3.7)	15.43	1.43	12.52	0.78	46.3	40.5	Y	PYYYY	
102	19124958-1550340	3.4 (3.8)	-34.1 (3.8)	-	-	11.85	0.55	44.3	-	P	PY-Y-	
103	19134512-1619340	19.9 (4.9)	-11.1 (4.9)	14.27	1.15	11.92	0.68	45.0	-	N	NY-YY	
104	19193779-1618312	11.4 (4.8)	-15.8 (4.8)	-	-	11.78	0.65	52.4	-	N	NN-Y-	
105	19181352-1614496	5.8 (3.7)	-58.2 (3.7)	14.39	1.16	11.87	0.68	50.5	-	N	NN-YY	
106	19163680-1623032	-3.0 (3.7)	-31.9 (3.7)	15.05	1.53	12.06	0.76	49.3	46.5	P	YPNYY	
107	19163732-1600050	-2.9 (3.7)	-34.8 (3.7)	14.70	1.26	12.02	0.66	42.5	42.1	Y	PYYYY	
108	19172940-1611577	9.1 (3.7)	-32.3 (3.7)	15.21	1.35	12.47	0.71	48.6	42.8	P	NPYYY	

Table 5 — Continued

CWW ID	2MASS ID	$\mu_{\text{RA}}(\sigma_{\mu})$	$\mu_{\text{Dec}}(\sigma_{\mu})$	g'	$g' - i'$	J ^a	$J - K_S$ ^a	RV _{LP}	RV _H	Mem. ^b	MemFlag ^c	Notes ^d
--------	----------	---------------------------------	----------------------------------	------	-----------	------------------	------------------------	------------------	-----------------	-------------------	----------------------	--------------------

Note. — Column Notes: (1) CWW ID – This work’s star identification scheme, sorted by V magnitude. CWW = Curtis, Wolfgang and Wright. (2) 2MASS ID, also provides RA and Dec positions (3, 4) RA and Dec proper motions in mas/yr from PPMXL catalog (5) CFHT/MegaCam g' mag. (6) $g' - i'$ mag. (7) 2MASS J mag. (8) 2MASS $J - K_S$ mag. (9) Lick / Palomar RV in km s⁻¹ (10) Hectochelle RV in km s⁻¹ (11) Membership probabilities (12) Membership probabilities for each criterion (13) Notes for individual stars. Vaues in parenthesis are measurement errors.

^a We use 2MASS aperture photometry instead of the default PSF photometry for 18 stars, based on our analysis that these stars, and only these stars, shift position on the ($J - K_S$) CMD and that they all move toward the cluster locus. No neighbors are resolved in our optical imaging within 5". The stars are CWW 22, 24, 27, 28, 30, 37, 38, 43, 48, 49, 57, 59, 67, 68, 90, 91, 94, and 100.

^b Membership Probability: Y = yes, highest confidence member, P = possible / probable member, N = not likely / non-member

^c Membership Criteria: proper motion radial distance from cluster value; Lick / Palomar RV, Hectochelle RV, 2MASS ($J - K_S$) CMD, CFHT/MegaCam ($g' - i'$) CMD. Confidence intervals defined in Table 2. A ‘B’ flag indicates photometry consistent with blue stragglers. A dash ‘-’ indicates no data.

^d Notes: BS = blue straggler, RG = red giant, SB2 = spectroscopic double line binary, SB1? = inconsistent RVs between multiple epochs

^e Our MegaCam imaging shows CWW 51 is an optical double, with a star 1.65" away with a similar $g' r' i' z'$ SED. Assuming a cluster distance of 300 pc, this angular separation translates into a minimum physical separation of 495 AU. This suggests that the pair actually form a wide binary, although their angular proximity could also be explained by a chance alignment. This double was not resolved in the 2MASS Point Source Catalog. Adding 0.75 mag. to the J band magnitude (halving the brightness, to reflect just the one star) moves CWW 51 in the ($J - K_S$) CMD to its neighbors in the ($g' - i'$) CMD. Despite this realization, we quote the 2MASS PSC photometry here. See §3.4.2.